Journal of Sound and Vibration 329 (2010) 2895–2914

Contents lists available at ScienceDirect

Journal of Sound and Vibration

journal homepage: www.elsevier.com/locate/jsvi

Role of spectrally varying mount properties in influencing coupling between powertrain motions under torque excitation

Jae-Yeol Park, Rajendra Singh *

Smart Vehicle Concepts Center and Acoustics and Dynamics Laboratory, The Ohio State University, Columbus, OH 43210, USA

ARTICLE INFO

Article history:
Received 23 September 2008
Received in revised form
26 January 2010
Accepted 28 January 2010
Handling Editor: M.P. Cartmell
Available online 21 February 2010

ABSTRACT

The influence of spectrally varying mount properties (including stiffness and damping) on the dynamics of powertrain motions is analytically examined. To overcome the deficiency of the direct inversion method (limited to only the frequency domain analysis), two methods are developed that describe the mount elements via a transfer function (in Laplace domain) or analogous mechanical model. New analytical formulations are verified by comparing the frequency responses with numerical results obtained by the direct inversion method (based on Voigt type mount model). Eigensolutions and transient responses of a spectrally varying mounting system are also predicted from new models. Based on complex eigenstructure, new coupling indices, including modal kinetic energy fractions, are defined for each method. Complex eigenvalue problem formulation with spectrally varying properties provides a closer match with measured natural frequencies than the real eigensolution with frequency-independent mounts. Given spectral variance in the mount properties, a simple roll mode decoupling scheme is suggested for the powertrain isolation system. Finally, an axiom for torque roll axis decoupling is provided by employing direct and adjoint eigenvalue problems.

1. Introduction

Prior analyses of rigid body isolation systems, including vibration transmissibility, natural frequency placement, and motion decoupling studies [1–7], assume that the stiffness (k) and viscous damping (c) properties are constant. However, real-life mount elements inherently (and some even by design) exhibit considerable frequency- and amplitude-dependency, express $k=k(\omega, x)$ and $c=c(\omega, x)$ where ω is the angular frequency (rad/s) and x is the amplitude of excitation [8–11]. The rigid body mounting systems are typically modeled in terms of a 6 degree of freedom (6-dof) inertial body that is supported by tri-axial isolation elements at 3 or 4 locations along with a rigid foundation [1–7]. Yu et al. [12], He and Singh [13], and Jeong and Singh [14] have suggested that it is necessary to incorporate the spectrally varying properties in the engine isolation system models. In this article, we attempt to fill this void in the literature and in particular examine the engine roll-mode decoupling scheme for such isolation systems. More specifically, we extend the work of Jeong and Singh [2] and Park and Singh [3], and focus on the effect of spectrally varying mount properties on engine motion coupling under torque excitation.

Jeong and Singh [14] had employed the Voigt type viscoelastic model given measured dynamic stiffness data (in frequency domain) and then conducted modal analyses of $\frac{1}{4}$ and $\frac{1}{2}$ vehicle models. However, the introduction of highly

* Corresponding author. Tel.: +1 614 292 9044; fax: +1 614 292 3163.
E-mail address: singh.3@osu.edu (R. Singh).

0022-460X/$ - see front matter © 2010 Elsevier Ltd. All rights reserved.
doi:10.1016/j.jsv.2010.01.031

frequency-dependent isolators requires a new analytical framework, especially for eigensolutions. The causality problem associated with the inverse Fourier transformation for frequency-dependent loss factor or viscous damping [14,15] is well-known, as physically unrealizable results that may emerge in time domain calculations. To overcome this difficulty, we assume that the characteristics of a supporting element are first identified in the Laplace domain, say in terms of the cross point dynamic stiffness using a non-resonant type experimental and/or analytical method [8,9]. Further, analogous mechanical models (such as those developed for the hydraulic engine mounts) could be utilized for analytical calculations (or dynamic design studies) under limited conditions [8,13]. Based on the above-mentioned mathematical description of mounts, we propose a new 6-dof rigid body mounting system model with $k_i(\omega)$ and $c_i(\omega)$ $i=1,\ldots,n$ where n is the number of tri-axial mount elements (with properties at a given excitation level). The governing system of this article is assumed to be linear time-invariant, though some mounts (hydraulic or adaptive type) could exhibit significant amplitude sensitivity.

2. Problem formulation

2.1. Physical system and frequency domain calculations (Method I)

Fig. 1 illustrates a typical rigid body isolation system composed of an inertial body (engine and transmission), a rigid base (chassis), and three or four mounts such that each isolation element could be arbitrarily placed at any exterior point and oriented in any direction. The dynamic characteristics of isolators are generally represented in terms of the complex-valued cross point dynamic stiffness, $K(\mathrm{j}\omega)=k(\omega)+\mathrm{j}c(\omega)$, from non-resonant dynamic test [8] where j is the imaginary unit. Fig. 2 shows sample measurements of $k(\omega)$ and $c(\omega)$ for two example cases (rubber and hydraulic engine mounts). We could embed these or similar $k_i(\omega)$ and $c_i(\omega)$ properties in one or more mount elements of Fig. 1. The governing equations of the mounting system in frequency domain (ω) are as follows, where $\mathbf{q}(\omega)$ is the dynamic displacement vector, and $\mathbf{f}(\omega)$ is the external excitation (force/torque) vector

$$[-\omega^2\mathbf{M}+\mathrm{j}\omega\mathbf{C}(\omega)+\mathbf{K}(\omega)]\mathbf{q}(\omega)=\mathbf{f}(\omega). \tag{1}$$

Here, $\mathbf{M}$ is the inertial (mass) matrix, and $\mathbf{K}(\omega)$ and $\mathbf{C}(\omega)$ are the stiffness and viscous damping matrices. For an internal combustion powertrain system, the main excitation, $\mathbf{f}(t)$, comes from the pulsating torque that is generated by multi-cylinder engines and it could be either periodic (under steady state) or transient (under start-up or switching conditions) [16–18]. Frequency responses could be numerically calculated by the direct inversion method (designated in this article as Method I), where we could simply use different k and c values at each frequency (essentially a look-up table scheme). However, Method I in Eq. (1) cannot directly lead to the analytical modal expansion for response predictions and motion coupling analyses. In order to overcome this limitation, Jeong and Singh [14] had formulated several spectral eigenvalue problems and then suggested modal superposition procedures. However, their method is valid for a special class of problems (where the dynamic stiffness is given in a specific form), and their approximation cannot be extended to a more general spectrally varying vibrating system.

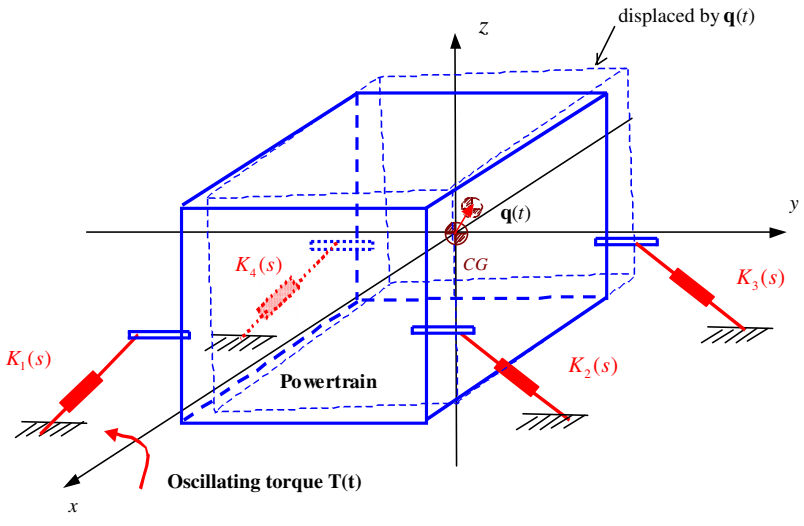

Fig. 1. Typical rigid body isolation system with mounts having spectrally varying stiffness and damping properties. Each mount is described by tri-axial elements with $k(\omega)$ and $c(\omega)$ properties. Here, $K_i(s)$ is the dynamic stiffness of the isolation element in a specific direction and CG is the center of gravity.

2.2. Transfer function model of frequency-dependent mounts (Method II)

The cross-point dynamic stiffness (in Laplace domain s) of a typical engine mount at a certain excitation amplitude, under a specific mean load, could be given by the following expression [8]:

$$K_i(s) = \frac{\alpha_b s^b + \cdots + \alpha_3 s^3 + \alpha_2 s^2 + \alpha_1 s + 1}{\beta_a s^a + \cdots + \beta_2 s^2 + \beta_1 s + \beta_0}. \tag{2}$$

Here, a and b are the order of denominator and numerator, respectively, and the coefficients, α_k and β_k, are determined by the experimental or numerical (analytical) method reflecting the internal fluid structure and rubber material properties. Observe that Eq. (2) matches well with the experimental results of Fig. 2 for hydraulic (with a=2, b=3) and rubber (with a=0, b=1) mounts. Employment of Eq. (2) to the powertrain mounts in Fig. 1 is designated here as Method II. This formulation could be used in time domain as well. When the coefficients in $K_i(s)$ are developed using measured data, they should be carefully employed to avoid the causality problem [19,20]. The necessary and sufficient condition for Eq. (2) to represent a causal system is that the real and imaginary parts of the $K_i(s)$ should form a Hilbert transform pair [21].

2.3. Analogous mechanical model of frequency-dependent mounts (Method III)

A real-life isolation device could be sometimes approximated by an equivalent mechanical or visco-elastic model under certain conditions [8,13,22]. For example, an analogous mechanical model of a highly frequency-dependent hydraulic mount is proposed [8,13] assuming a fixed base at one end. With a linearized approximation around the operating point(s), over the lower frequency range, the dynamic stiffness is approximated as

$$K_i(s) = \frac{\alpha_3 s^3 + \alpha_2 s^2 + \alpha_1 s + 1}{\beta_2 s^2 + \beta_1 s + \beta_0} \approx k_r + c_r s + k_M - \frac{k_M^2}{m_M s^2 + c_M s + k_M}. \tag{3}$$

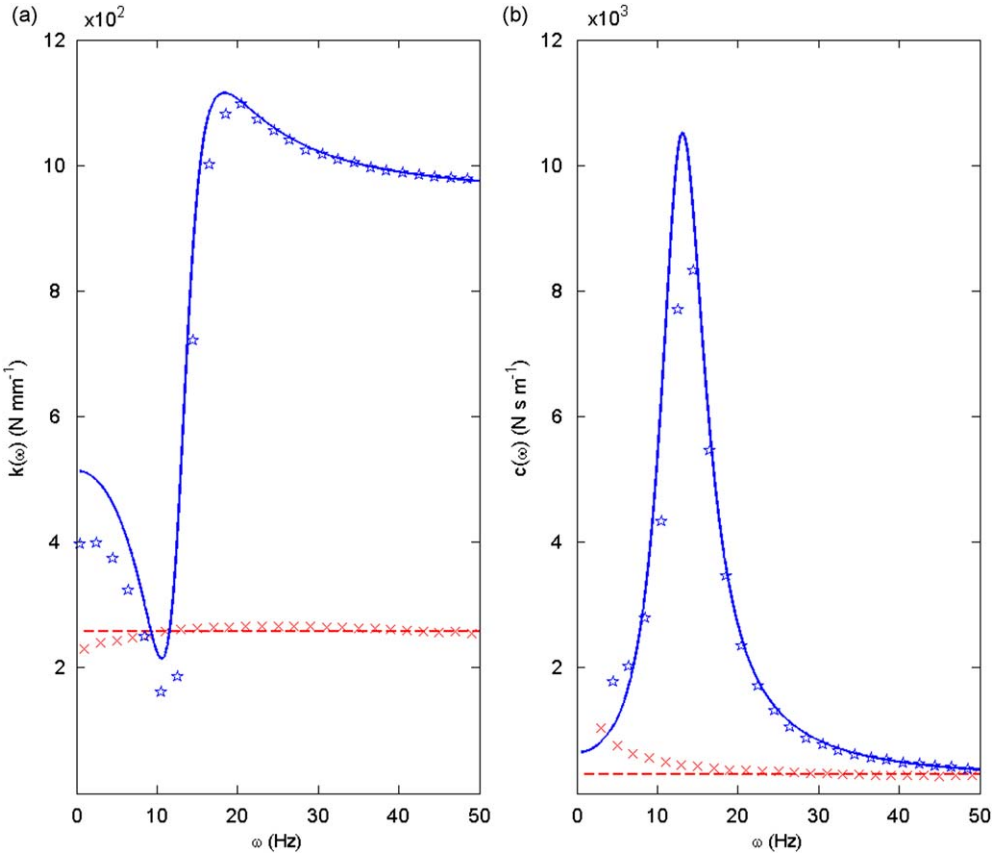

Fig. 2. Mount examples with spectrally varying stiffness and viscous damping properties. Measured data for rubber and hydraulic mounts are compared, respectively, with transfer function (TF) models given by Eq. (2). (a) Stiffness spectra, $k(\omega) = \mathrm{Re}[K(\mathrm{j}\omega)]$; (b) viscous damping spectra, $c(\omega) = \mathrm{Im}[K(\mathrm{j}\omega)]/\omega$. Key: ☆, measured data for a hydraulic mount with an excitation amplitude of x=1.5 mm; ×, measured data for a rubber mount; ▬, second-order TF for the hydraulic mount; ▬ ▬, zeroth-order TF for the rubber mount (k=280 N mm^{-1}, and c=300 N s m^{-1}).

Fig. 3 shows the results for the hydraulic mount corresponding to Eq. (3) along with the Voigt type visco-elastic model for a rubber mount; refer to the figure for symbols and parameters. Such mechanical models are designated under Method III; dynamic solutions from this procedure will be compared with Methods I and II (direct inversion and transfer function formulations).

2.4. Objectives

The first objective is to extend the work of Jeong and Singh [2] and Park and Singh [3], and develop an analytical rigid body mounting system model with $k(\omega)$and $c(\omega)$ elements based on the transfer function formulation or equivalent mechanical model as suggested by Eq. (2) or (3). Based on Methods II and III (analytically developed in Sections 3 and 4, respectively), complex eigensolutions are calculated and applied to predict frequency and time responses using the modal superposition method. The proposed methods are verified in frequency domain, under the harmonic torque excitation, by comparison with the direct inversion method based on Eq. (1). The second objective is to study the influence of $k(\omega)$ and $c(\omega)$ on powertrain motion coupling; this is accomplished by developing modal scalar functions based on complex eigensolutions. A simple (2-D) engine roll-mode decoupling scheme is then suggested, and an axiom for 3-D TRA decoupling is provided; this will extend the work of Park and Singh [3]. Finally, the three methods are quantitatively and qualitatively compared in terms of eigensolutions and motion coupling issues. An overview of three methods is given in Table 1.

3. Analytical development of Method II

The following three coordinate systems are used in this article: inertial coordinates $(XYZ)_g$, local mount coordinates $(XYZ)_{mi}$ parallel with $(XYZ)_g$, and principal mount direction coordinates $(XYZ)_{mpi}$ whose principal axes are not parallel with

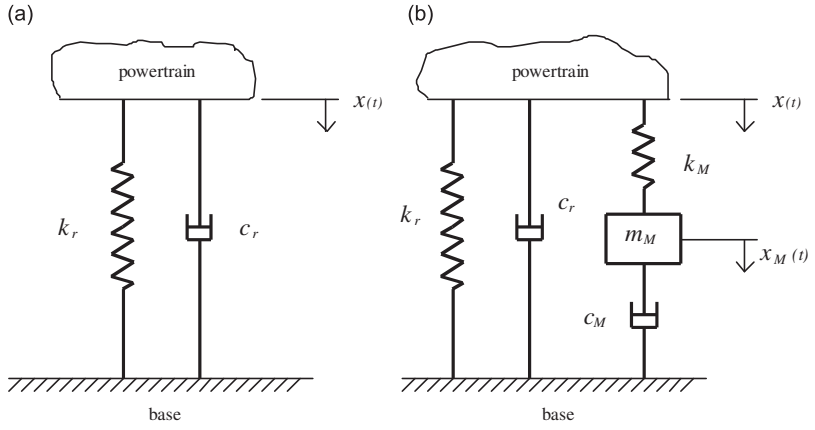

Fig. 3. Analogous mechanical models of rubber and hydraulic mounts. (a) Rubber mount (Voigt type model) and (b) hydraulic mount. Note that the fixed base is assumed for such models.

Table 1
Summary of three methods for the rigid body isolation system with $k(\omega)$ and $c(\omega)$ properties. Refer to the text for symbols.

	Method I (direct inversion)	Method II (transfer function)	Method III (mechanical model)
Governing equations in ω domain	$[-\omega^2\mathbf{M}+\mathrm{j}\omega\mathbf{C}+\mathbf{K}]\mathbf{q}(\omega)=\mathbf{f}(\omega)$ (dimension or dof=6)	Same	Same
Governing equations in t domain	Not formulated	$\mathbf{M}_e\ddot{\mathbf{q}}_e(t)+\mathbf{C}_e\dot{\mathbf{q}}_e(t)+\mathbf{K}_e\mathbf{q}_e(t)=\mathbf{f}_e(t)$ (dimension=$6+N_{hdr}$)	$\mathbf{M}_{Me}\ddot{\mathbf{q}}_{Me}(t)+\mathbf{C}_{Me}\dot{\mathbf{q}}_{Me}(t)+\mathbf{K}_{Me}\mathbf{q}_{Me}(t)=\mathbf{f}_{Me}(t)$ (dimension=$6+N_{hdr}$)
Nature of system matrices	Symmetric	Asymmetric	Symmetric
Complex eigenvalue problem	Not defined	$\begin{cases}\lambda_r\mathbf{A}\mathbf{U}_r+\mathbf{B}\mathbf{U}_r=\mathbf{0}\\ \lambda_r\mathbf{A}\mathbf{V}_r+\mathbf{B}\mathbf{V}_r=\mathbf{0}\end{cases}$	$\lambda_{Mr}\mathbf{A}_M\mathbf{U}_{Mr}+\mathbf{B}_M\mathbf{U}_{Mr}=\mathbf{0}$
Orthogonality of complex modes	Not defined	$\begin{cases}\mathbf{V}_r^{\mathrm{T}}\mathbf{A}\mathbf{U}_s=\delta_{rs}\\ \mathbf{V}_r^{\mathrm{T}}\mathbf{B}\mathbf{U}_s=-\lambda_r\delta_{rs}\end{cases}$	$\begin{cases}\mathbf{U}_{Mr}^{\mathrm{T}}\mathbf{A}_M\mathbf{U}_{Ms}=\delta_{rs}\\ \mathbf{U}_{Mr}^{\mathrm{T}}\mathbf{B}_M\mathbf{U}_{Ms}=-\lambda_{Mr}\delta_{rs}\end{cases}$
Modal expansion (for complex modes)	Not valid	Valid	Valid
Modal kinetic energy fraction: $\xi_{X_i,\omega_r}(=KE_{X_i,\omega_r}/KE_{\omega_r})$	Not defined	$\begin{cases}KE_{X_i,\omega_r}=(1/2)m_i\omega_r^2\lvert[\mathbf{u}_r]_{X_i}\rvert^2\\ KE_{\omega_r}=(1/2)\omega_r^2\lvert\mathbf{u}_r^{\mathrm{T}}\mathbf{M}_e\mathbf{u}_r\rvert\end{cases}$	$\begin{cases}KE_{X_i,\omega_r}=(1/2)m_i\omega_r^2\lvert[\mathbf{u}_{Mr}]_{X_i}\rvert^2\\ KE_{\omega_r}=(1/2)\omega_r^2\lvert\mathbf{u}_{Mr}^{\mathrm{T}}\mathbf{M}_{Me}\mathbf{u}_{Mr}\rvert\end{cases}$

$(XYZ)_g$, $i=1, \ldots, n$ where n is the number of mounts. The $(\mathrm{i})_g$ coordinate system is a ground-fixed reference frame with its origin at static equilibrium (at the center of gravity, CG). The displacement vector of the inertial body is expressed by the translational and angular displacements of the center of gravity (CG), and is given by $\mathbf{q}(t)=[x\ y\ z\ \theta_x\ \theta_y\ \theta_z]^{\mathrm{T}}(t)$. The governing equations of motion are formulated in matrix form, as shown below for small amplitudes, where $\dot{\mathbf{q}}(t)$ and $\ddot{\mathbf{q}}(t)$ are the velocity and acceleration vectors, respectively of dimension N (=6)

$$\mathbf{M}\ddot{\mathbf{q}}(t)+\mathbf{C}\dot{\mathbf{q}}(t)+\mathbf{K}\mathbf{q}(t)=\mathbf{f}(t)+\mathbf{r}_{fd}(t). \tag{4}$$

Here, $\mathbf{M}$ is the inertial (mass) matrix, $\mathbf{K}$ is the stiffness matrix, $\mathbf{C}$ is the viscous damping matrix, $\mathbf{f}(t)$ is the external excitation (force/torque) vector, and $\mathbf{r}_{fd}(t)$ is the reaction force from the frequency-dependent components. The method for incorporating the stiffness and damping matrices from the local mounts has been well-described by Park and Singh [3]. Express the reaction force, $\mathbf{r}_{fd}(t)$, as the sum of forces from N_{fd} number of frequency-dependent components

$$\mathbf{r}_{fd}(t)=\sum_{k=1}^{N_{fd}}\mathbf{r}_{fd,k}(t). \tag{5}$$

The transfer function model for the k-th frequency-dependent mount is as follows, where $\mathcal{L}$ is the symbol of Laplace transform, and $r_{fd,k}(t)$ and $x_{fd,k}(t)$ are output force and input displacement, respectively, in a specific direction of an isolation element

$$K_{fd,k}(s)=\frac{R_{fd,k}(s)}{X_{fd,k}(s)}=\frac{\mathcal{L}[r_{fd,k}(t)]}{\mathcal{L}[x_{fd,k}(t)]},\quad k=1,2,\ \ldots,N_{fd}. \tag{6}$$

The local reaction force for the k-th mount, $r_{fd,k}(t)$, is represented in the global $(XYZ)_g$ coordinates by using the kinematics in terms of the orientation angles and locations of mounts while the input displacement, $x_{fd,k}(t)$, is also found based on the geometry in the rigid body mounting system. Since the displacements at the mount location(s) caused by the rigid body rotations are computed by using a cross vector product, the resulting deflection, $\mathbf{q}_{mi}(t)$, at each mount is as follows based on the rigid base assumption:

$$\mathbf{q}_{mi,t}(t)=\mathbf{q}_t(t)+\mathbf{q}_\theta(t)\times\mathbf{r}_{mi}, \tag{7}$$

in which $\mathbf{r}_{mi}=[r_{xi}r_{yi}r_{zi}]^{\mathrm{T}}$ is the position vector of each mount and $\mathbf{q}_t(t)=[XYZ]^{\mathrm{T}}(t)$ and $\mathbf{q}_\theta(t)=[\theta_X\theta_Y\theta_Z]^{\mathrm{T}}(t)$ are the translational and rotational displacements of the rigid body. The cross vector in Eq. (7) can be expressed by a tensor skew matrix, $\mathbf{L}_{mi}$

$$\mathbf{q}_{mi,t}(t)=\begin{bmatrix}\mathbf{I} & \mathbf{L}_{mi}\end{bmatrix}\mathbf{q}(t), \tag{8}$$

$$\mathbf{L}_{mi}=\begin{bmatrix}0 & r_{zi} & -r_{yi}\\ & 0 & r_{xi}\\ \textit{skew sym.} & & 0\end{bmatrix}. \tag{9}$$

The displacement, $\mathbf{q}_{\mathrm{mp}i}(t)$, of the i-th mount with respect to the principal mount direction coordinates, $(XYZ)_{\mathrm{mp}i}$, is expressed as follows:

$$\mathbf{q}_{\mathrm{mp}i}(t)=\begin{bmatrix}\mathbf{q}_{\mathrm{mp}i,t}(t)\\ \mathbf{q}_{\mathrm{mp}i,\theta}(t)\end{bmatrix}=\mathbf{\Theta}_{\mathrm{g,m}i}^{\mathrm{T}}\begin{bmatrix}\mathbf{I} & \mathbf{L}_{\mathrm{m}i}\\ 0 & \mathbf{I}\end{bmatrix}\mathbf{q}(t). \tag{10}$$

Here, $\mathbf{q}_{\mathrm{mp}i,\theta}(t)$ is the displacement vector at i-th mount contributed by the rotational motion of powertrain $\mathbf{q}_\theta(t)$. The rotational matrix, $\mathbf{\Theta}_{g,\mathrm{m}i}$, for i-th mount is derived from the orientation angles of each mount and by rotating the local $(XYZ)_{\mathrm{m}i}$ coordinate system at each mount about the global $(XYZ)_g$ axes sequentially for X, Y, and Z. On the other hand, the reaction force in the i-th mount in the global coordinate is obtained by a transformation from the local mount coordinates, and the resulting reaction forces are

$$\mathbf{f}_{\mathrm{g,m}i}(t)=\begin{bmatrix}\mathbf{f}_{\mathrm{g,m}i,\mathrm{t}}(t)\\ \mathbf{f}_{\mathrm{g,m}i,\theta}(t)\end{bmatrix}=\begin{bmatrix}\mathbf{f}_{\mathrm{m}i,t}(t)\\ \mathbf{r}_{\mathrm{m}i}\times\mathbf{f}_{\mathrm{m}i,t}(t)\end{bmatrix}=\begin{bmatrix}\mathbf{I}\\ \mathbf{L}_{\mathrm{m}i}^{\mathrm{T}}\end{bmatrix}\mathbf{f}_{\mathrm{m}i,t}(t). \tag{11}$$

Since $\mathbf{f}_{\mathrm{m}i,t}(t)=\mathbf{\Theta}_{g,\mathrm{m}i}\mathbf{f}_{\mathrm{mp}i,t}(t)$, Eq. (11) becomes

$$\mathbf{f}_{\mathrm{g,m}i}(t)=\begin{bmatrix}\mathbf{I}\\ \mathbf{L}_{\mathrm{m}i}^{\mathrm{T}}\end{bmatrix}\mathbf{\Theta}_{\mathrm{g,m}i}\mathbf{f}_{\mathrm{mp}i,t}(t). \tag{12}$$

Based on the fact that the output reaction force, $r_{fd,k}(t)$, is described in the $(XYZ)_{\mathrm{mp}i}$ coordinates as $\mathbf{f}_{fd,k-\mathrm{mp}i}(t)=\begin{bmatrix}r_{fd,k}(t) & 0 & 0\end{bmatrix}^{\mathrm{T}}$, its transformation ($\mathbf{r}_{fd,k}(t)$) to the global coordinate system is expressed using Eq. (12) as

$$\mathbf{r}_{fd,k}(t)=\mathbf{f}_{fd,k-g,\mathrm{m}i}(t)=\begin{bmatrix}\mathbf{I}\\ \mathbf{L}_{\mathrm{m}i}^{\mathrm{T}}\end{bmatrix}\mathbf{\Theta}_{g,\mathrm{m}i}\begin{bmatrix}r_{fd,k}(t)\\ 0\\ 0\end{bmatrix}. \tag{13}$$

Since the input displacement, $x_{fd,k}(t)$, to a frequency-dependent element from rigid body motion ($\mathbf{q}(t)$) is set as one of the principal directions of i-th mount component, $x_{fd,k}(t)$ is obtained by finding a corresponding vector element in $\mathbf{q}_{\mathrm{mp}i}(t)$ of Eq. (10) as follows:

$$x_{fd,k}(t)=\mathbf{q}_{\mathrm{mp}i,v}(t), \quad v=x \text{ or } y \text{ or } z. \tag{14}$$

The resulting input displacement in the direction of spectrally varying mount is now completely described in terms of the orientation angle, its location, and rigid body motion without adding another variable for itself.

Next, the general form of mount transfer function, Eq. (2), can be readily used in the following procedure. To illustrate our method, we consider the hydraulic mount example that shows considerable frequency-dependency [8]. This is modeled in terms of only one pole and b zeros (sufficient at lower frequencies) as shown below

$$K_{fd,k}(s)=\frac{\alpha_{b,k}s^b+\cdots+\alpha_{1,k}s+1}{\beta_{2,k}s^2+\beta_{1,k}s+\beta_{0,k}}, \tag{15}$$

where the numerator order b could be either 2, 3, or 4, depending on the desired accuracy [8]. We apply the inverse Laplace transform to obtain the time domain formulation

$$\mathrm{h}_k(t)=\mathbf{b}_{fd,k}(t), \quad k=1,\,2,\,\ldots,\,N_{fd}, \tag{16}$$

in which

$$\mathbf{h}_k(t)=\mathcal{L}^{-1}[(\alpha_{b,k}s^b+\cdots+\alpha_{1,k}s+1)X_{fd,k}(s)], \tag{17a}$$

$$\mathbf{b}_{fd,k}(t)=\mathcal{L}^{-1}[(\beta_{2,k}s^2+\beta_{1,k}s+\beta_{0,k})R_{fd,k}(s)], \tag{17b}$$

By transforming the governing equations, Eq. (16), to the global coordinate system by using the kinematic relationships given by Eqs. (13) and (14), we get

$$\mathbf{h}_k(t)=\mathbf{b}_{fd,k}(t), \quad k=1,2,\,\ldots,\,N_{fd}. \tag{18}$$

Note that the reaction forces, $r_{fd,k}(t)$, introduce additional vector elements in $\mathbf{q}(t)$ in the following form due to frequency-dependent components

$$\mathbf{q}_e(t)=\begin{bmatrix}\mathbf{q}^{\mathrm{T}}(t) & \mathbf{f}_{fd}^{\mathrm{T}}(t)\end{bmatrix}^{\mathrm{T}}, \tag{19a}$$

$$\mathbf{f}_{fd}(t)=\begin{bmatrix}r_{fd,1}(t) & \ldots & r_{fd,N_{fd}}(t)\end{bmatrix}^{\mathrm{T}}. \tag{19b}$$

Thus, the dynamics of the spectrally varying mounting system is represented in an extended form. Here, note that if each mount has one pole in the transfer function, we will have $N+N_{fd}$ equations since one inertial element is brought in by each mount. For an asymmetric mounting system, Eqs. (3) and (18) are expanded using the kinematics developed above as follows:

$$m\ddot{x}(t)+\mathbf{c}_{mx}^{\mathrm{T}}\dot{\mathbf{q}}(t)+\mathbf{k}_{mx}^{\mathrm{T}}\mathbf{q}(t)=f_x+f_{rx}(r_{fd,1},\,\ldots,\,r_{fd,N_{fd}}), \tag{20a}$$

$$m\ddot{y}(t)+\mathbf{c}_{my}^{\mathrm{T}}\dot{\mathbf{q}}(t)+\mathbf{k}_{my}^{\mathrm{T}}\mathbf{q}(t)=f_y+f_{ry}(r_{fd,1},\,\ldots,\,r_{fd,N_{fd}}), \tag{20b}$$

$$m\ddot{z}(t)+\mathbf{c}_{mz}^{\mathrm{T}}\dot{\mathbf{q}}(t)+\mathbf{k}_{mz}^{\mathrm{T}}\mathbf{q}(t)=f_z+f_{rz}(r_{fd,1},\,\ldots,\,r_{fd,N_{fd}}), \tag{20c}$$

$$I_{xx}\ddot{\theta}_x(t)+I_{xy}\ddot{\theta}_y(t)+I_{xz}\ddot{\theta}_z(t)+\mathbf{c}_{m\theta_x}^{\mathrm{T}}\dot{\mathbf{q}}(t)+\mathbf{k}_{m\theta_x}^{\mathrm{T}}\mathbf{q}(t)=M_x+M_{r\theta_x}(r_{fd,1},\,\ldots,\,r_{fd,N_{fd}}), \tag{20d}$$

$$I_{xy}\ddot{\theta}_x(t)+I_{yy}\ddot{\theta}_y(t)+I_{yz}\ddot{\theta}_z(t)+\mathbf{c}_{m\theta_y}^{\mathrm{T}}\dot{\mathbf{q}}(t)+\mathbf{k}_{m\theta_y}^{\mathrm{T}}\mathbf{q}(t)=M_y+M_{r\theta_y}(r_{fd,1},\,\ldots,\,r_{fd,N_{fd}}), \tag{20e}$$

$$I_{xz}\ddot{\theta}_x(t)+I_{yz}\ddot{\theta}_y(t)+I_{zz}\ddot{\theta}_z(t)+\mathbf{c}_{m\theta_z}^{\mathrm{T}}\dot{\mathbf{q}}(t)+\mathbf{k}_{m\theta_z}^{\mathrm{T}}\mathbf{q}(t)=M_z+M_{r\theta_z}(r_{fd,1},\,\ldots,\,r_{fd,N_{fd}}), \tag{20f}$$

$$\mathrm{h}_k(x_{fd,k}^{(b)}(t),\,\ldots,\,x_{fd,k}(t))=\mathrm{b}_k(r_{fd,1}^{(2)},\,\ldots,\,r_{fd,1},\,\ldots,\,r_{fd,N_{fd}}^{(2)},\,\ldots,\,r_{fd,N_{fd}}), \quad k=1,\,2,\,\ldots,\,N_{fd}. \tag{20g}$$

Combining Eqs. (20a–g) with zero initial conditions in the inverse Laplace transform in Eq. (20g), we assemble the "extended" governing equations (in matrix form) for the mounting system with frequency-dependent components as follows:

$$\mathbf{M}_e\ddot{\mathbf{q}}_e(t)+\mathbf{C}_e\dot{\mathbf{q}}_e(t)+\mathbf{K}_e\mathbf{q}_e(t)=\mathbf{f}_e(t). \tag{21}$$

Here,

$$\mathbf{M}_e=\begin{bmatrix}\mathbf{M} & \mathbf{0}\\ \mathbf{0} & \mathbf{M}_{fd}\end{bmatrix},\quad \mathbf{C}_e=\begin{bmatrix}\mathbf{C} & \mathbf{C}_{fd,1}\\ \mathbf{C}_{fd,2} & \mathbf{C}_{fd,3}\end{bmatrix},\quad \mathbf{K}_e=\begin{bmatrix}\mathbf{K} & \mathbf{K}_{fd,1}\\ \mathbf{K}_{fd,2} & \mathbf{K}_{fd,3}\end{bmatrix}, \tag{22a,b,c}$$

$$\mathbf{f}_e(t)=\begin{bmatrix}\mathbf{f}^{\mathrm{T}}(t) & \boldsymbol{\sigma}_{fd}^{\mathrm{T}}(t)\end{bmatrix}^{\mathrm{T}}=\begin{bmatrix}\mathbf{f}^{\mathrm{T}}(t) & \sigma_{fd,1}(t) & \dots & \sigma_{fd,N_{fd}}(t)\end{bmatrix}^{\mathrm{T}}. \tag{22d}$$

The extended matrices of Eq. (21), $\mathbf{M}_e$, $\mathbf{C}_e$, and $\mathbf{K}_e$, include sub-matrices and the original matrices, $\mathbf{M}$, $\mathbf{C}$, and $\mathbf{K}$. The dimension of the matrices with frequency-dependent mounts is now $(N+N_{fd})\times(N+N_{fd})$, while $N\times N$ is the dimension with spectrally invariant properties. Observe that the extended matrices are no longer frequency-dependent, as they contain constant values as shown above. Further, they are not symmetric matrices due to asymmetry in the expanded parts. Therefore, it is now possible to define an appropriate eigenvalue problem for asymmetric matrices as discussed in the Section 5.

4. Analytical development of Method III

Based on the parameters of Eq. (3), we can assemble the governing equations for the isolation system with mechanical models of mounts. The reaction force from the k-th hydraulic mount of Fig. 3(b), $r_{Mfd,k}(t)$, is formulated as

$$r_{Mfd,k}(t)=k_{r,k}x_{fd,k}(t)+c_{r,k}\dot{x}_{fd,k}(t)+k_{M,k}[x_{fd,k}(t)-x_{M,k}(t)]. \tag{23}$$

Using Eq. (14), Eq. (23) is rewritten as

$$r_{Mfd,k}(t)=k_{r,k}\mathbf{q}_{mpi,v}(t)+c_{r,k}\mathbf{q}_{mpi,v}(t)+k_{M,k}[\mathbf{q}_{mpi,v}(t)-x_{M,k}(t)]. \tag{24}$$

We formulate its vector form, $\mathbf{r}_{Mfd,k}(t)$, by substituting Eq. (24) in Eq. (13), and the sum of reaction forces, $\mathbf{r}_{Mfd}(t)$, is obtained for all frequency-dependent components. We obtain the following governing equations (essentially Eq. (4) with additional independent variables $x_{M,k}(t)$):

$$\mathbf{M}\ddot{\mathbf{q}}(t)+\mathbf{C}\dot{\mathbf{q}}(t)+\mathbf{K}\mathbf{q}(t)=\mathbf{f}(t)+\mathbf{r}_{Mfd}(t). \tag{25}$$

For the inertial mass ($m_{M,k}$) of k-th hydraulic mount, the governing equation is

$$m_{M,k}\ddot{x}_{M,k}(t)+c_{\mathrm{M},k}\dot{x}_{M,k}(t)-k_{M,k}[\mathbf{q}_{mpi,t_p}(t)-x_{M,k}(t)]=0. \tag{26}$$

Combining Eqs. (25) and (26), we formulate yet another set of extended equations (in a matrix form) for a rigid body mounting system with frequency-dependent components as follows:

$$\mathbf{M}_{Me}\ddot{\mathbf{q}}_{Me}(t)+\mathbf{C}_e\dot{\mathbf{q}}_{Me}(t)+\mathbf{K}_{Me}\mathbf{q}_{Me}(t)=\mathbf{f}_{Me}(t). \tag{27}$$

Here,

$$\mathbf{M}_{Me}=\begin{bmatrix}\mathbf{M} & \mathbf{0}\\ \text{sym.} & \mathbf{M}_M\end{bmatrix},\quad \mathbf{C}_{Me}=\begin{bmatrix}\mathbf{C} & \mathbf{C}_{M,1}\\ \text{sym.} & \mathbf{C}_{M,2}\end{bmatrix},\quad \mathbf{K}_{Me}=\begin{bmatrix}\mathbf{K} & \mathbf{K}_{M,1}\\ \text{sym.} & \mathbf{K}_{M,2}\end{bmatrix}, \tag{28a,b,c}$$

$$\mathbf{q}_{Me}(t)=\begin{bmatrix}\mathbf{q}^{\mathrm{T}}(t) & \mathbf{x}_M^{\mathrm{T}}(t)\end{bmatrix}^{\mathrm{T}}=\begin{bmatrix}\mathbf{q}^{\mathrm{T}}(t) & x_{M,1}(t) & \dots & x_{M,N_{\mathrm{fd}}}(t)\end{bmatrix}. \tag{28d}$$

$$\mathbf{f}_{Me}(t)=\begin{bmatrix}\mathbf{f}^{\mathrm{T}}(t) & \mathbf{0}^{\mathrm{T}}(t)\end{bmatrix}^{\mathrm{T}}=\begin{bmatrix}\mathbf{f}^{\mathrm{T}}(t) & 0 & \dots & 0\end{bmatrix}^{\mathrm{T}}. \tag{28e}$$

Note that Eq. (27) with the mechanical model is a simplified version of Eq. (21), which was obtained using the transfer function model. In fact, this result is expected from a linearized approximation of a damped mechanical model based on the transfer function formulation. If Eq. (27) is sufficiently accurate to describe the transfer function model, it would be more convenient to use for modal and forced response analyses.

5. Verification of Methods II and III

5.1. Modal solutions and analytical frequency responses using Method II

The governing equations of Method I (with asymmetric $\mathbf{K}_e$ and $\mathbf{C}_e$) are now represented in state-space form as

$$\mathbf{A}\dot{\mathbf{p}}(t)+\mathbf{B}\mathbf{p}(t)=\mathbf{g}(t), \tag{29}$$

$$\mathbf{A}=\begin{bmatrix}\mathbf{M}_e & \mathbf{0}\\ \mathbf{0} & -\mathbf{K}_e\end{bmatrix},\quad \mathbf{B}=\begin{bmatrix}\mathbf{C}_e & \mathbf{K}_e\\ \mathbf{K}_e & \mathbf{0}\end{bmatrix},\quad \mathbf{p}(t)=\begin{bmatrix}\dot{\mathbf{q}}_e(t)\\ \mathbf{q}_e(t)\end{bmatrix},\quad \mathbf{g}(t)=\begin{bmatrix}\mathbf{f}_e(t)\\ \mathbf{0}\end{bmatrix}. \tag{30a,b,c,d}$$

Since the system matrices, **A** and **B**, are not self-adjoint, the direct (right) and adjoint (left) eigenvalue problems are formulated from Eq. (29) as follows:

$$\lambda\mathbf{AU}+\mathbf{BU}=\mathbf{0} \text{ and } \lambda\mathbf{A}^{\mathrm{T}}\mathbf{V}+\mathbf{B}^{\mathrm{T}}\mathbf{V}=\mathbf{0}. \tag{31a,b}$$

Here, **U** and **V** are the direct (right) and adjoint (left) eigenvectors, respectively, and λ is the eigenvalue [23]. They are described by the following:

$$\mathbf{U}=\begin{bmatrix}\lambda\mathbf{u}\\ \mathbf{u}\end{bmatrix} \text{ and } \mathbf{V}=\begin{bmatrix}\lambda\mathbf{v}\\ \mathbf{v}\end{bmatrix}. \tag{32a,b}$$

Next, we employ the eigensolutions for the calculation of frequency response by using biorthogonal properties [23]: $\mathbf{V}_r^{\mathrm{T}}\mathbf{A}\mathbf{U}_s=\delta_{rs}$, $\mathbf{V}_r^{\mathrm{T}}\mathbf{B}\mathbf{U}_s=-\lambda_r\delta_{rs}$, r, s=1, 2, 3, …, $2(N+N_{fd})$ where δ_{rs} is the Kroneker delta function. Assuming harmonic excitation as $\mathbf{g}(t)=\mathbf{G}e^{j\omega t}$, we analytically predict the frequency response as follows:

$$\mathbf{p}(t)=\mathbf{U}^{\mathrm{T}}(j\omega\mathbf{I}-\mathbf{\Lambda})\mathbf{V}\mathbf{G}e^{j\omega t}, \tag{33}$$

in which,

$$\mathbf{U}=\begin{bmatrix}\mathbf{u}_1 & \mathbf{u}_2 & \cdots & \mathbf{u}_{2(N+N_{fd})-1} & \mathbf{u}_{2(N+N_{fd})}\end{bmatrix}, \tag{34a}$$

$$\mathbf{V}=\begin{bmatrix}\mathbf{v}_1 & \mathbf{v}_2 & \cdots & \mathbf{v}_{2(N+N_{fd})-1} & \mathbf{v}_{2(N+N_{fd})}\end{bmatrix}, \tag{34b}$$

$$\mathbf{\Lambda}=\mathrm{diag}\left(\begin{bmatrix}\lambda_1 & \lambda_2 & \cdots & \lambda_{2(N+N_{fd})-1} & \lambda_{2(N+N_{fd})}\end{bmatrix}\right). \tag{34c}$$

5.2. Verification of Methods II and III

For the verification of Method II, the analytical frequency responses using complex eigensolution will be compared with the ones obtained using Method I (direct inversion method with a look-up table for frequency-dependent stiffness and

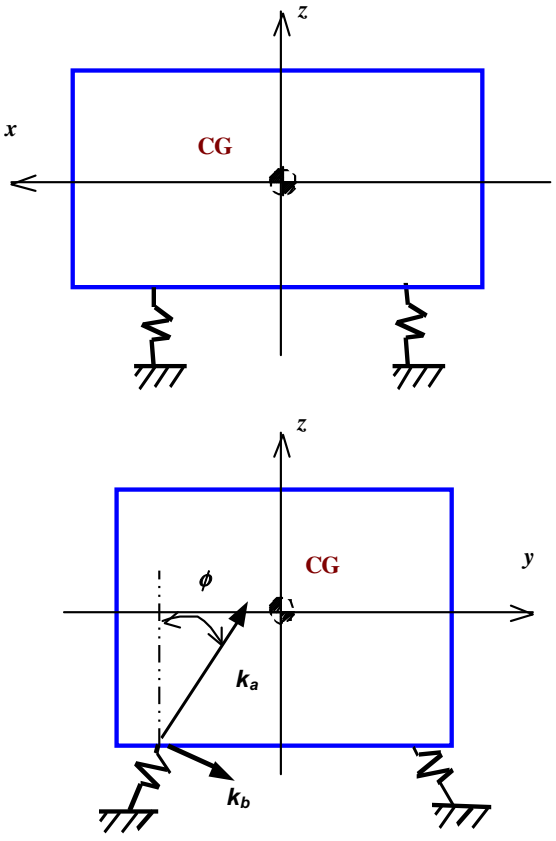

Fig. 4. Focalized powertrain mounting system (6-dof). Here, k_a is the principal compressive stiffness and k_b is the principal shear stiffness.

damping) for a simple focalized rigid body mounting system as shown in Figs. 1 and 4. The parameters are as follows: mass $m=100.5\,\mathrm{kg}$; moment of inertia ($\mathrm{kg\,m^2}$) $I_{XX}=1.65$, $I_{YY}=2.43$, $I_{ZZ}=2.54$; inertia product ($\mathrm{kg\,m^2}$) $I_{XY}=I_{XZ}=I_{YZ}=0$. Stiffness and damping coefficients of the rubber mounts (using the Voigt model) are: stiffness $k_a=280\,\mathrm{N\,mm^{-1}}$; stiffness rate ratio $L_k(=k_a/k_b)=2.5$; damping $c_a=30\,\mathrm{N\,s\,m^{-1}}$; damping rate ratio $L_c(=c_a/c_b)=2.5$; mount orientation $\phi=30^\circ$; mount locations in x-direction $r_{x,1}=r_{x,2}=318\,\mathrm{mm}$, $r_{x,3}=r_{x,4}=-318\,\mathrm{mm}$; mount locations in y-direction $r_{y,1}=r_{y,3}=-198\,\mathrm{mm}$, $r_{y,2}=r_{y,4}=198\,\mathrm{mm}$; mount locations in z-direction $r_{z,1}=r_{z,2}=r_{z,3}=r_{z,4}=-94\,\mathrm{mm}$. A highly frequency-dependent hydraulic mount of Fig. 2 is now placed at one location (say #1). The mount parameters are given in terms of its mechanical model: $k_r=512.95\,\mathrm{N\,mm^{-1}}$, $c_r=198\,\mathrm{N\,s\,m^{-1}}$, $m_M=62.8\,\mathrm{kg}$, $c_M=2666\,\mathrm{N\,s\,m^{-1}}$, and $k_M=436.95\,\mathrm{N\,m^{-1}}$. Fig. 5 compares frequency responses (given harmonic torque) for the three methods; an exact match is seen. This result validates the proposed rigid body mounting system model with frequency-dependent mounts described by either the transfer function or the analogous mechanical model. Observe that the resonant frequencies differ from those obtained when we apply mount model with contact k and c values. Next, we examine the modes of a V6 diesel engine isolation system [6]. In Table 2, measured natural frequencies (from Ref. [6]) are compared with two sets of natural frequency calculations: (i) real eigensolutions with spectrally invariant stiffness and viscous damping, and (ii) complex eigensolutions with spectrally varying stiffness and viscous damping properties (as shown in Fig. 6) only at mount #1 location. We observe a closer agreement with the measured values when the calculation includes frequency-dependent mount properties. This suggests that the spectrally varying support elements must be included for accurate isolation performance studies. Detailed eigenvalue analysis is presented in the next section.

In this focalized mounting system, the torque roll axis (TRA) decoupling is achieved with proportional damping, and there is only a roll response given the torque excitation shown in Fig. 7. However, when the damping is increased by a factor of 10 at location #1 ($10c_a$), coupled motions are seen in Fig. 7. It is observed that more significant coupling takes place with the use of a frequency-dependent mount at the same place (#1). In order to avoid the above motion coupling by frequency-dependence, it is desirable to find the TRA decoupling scheme under spectrally varying mounts.

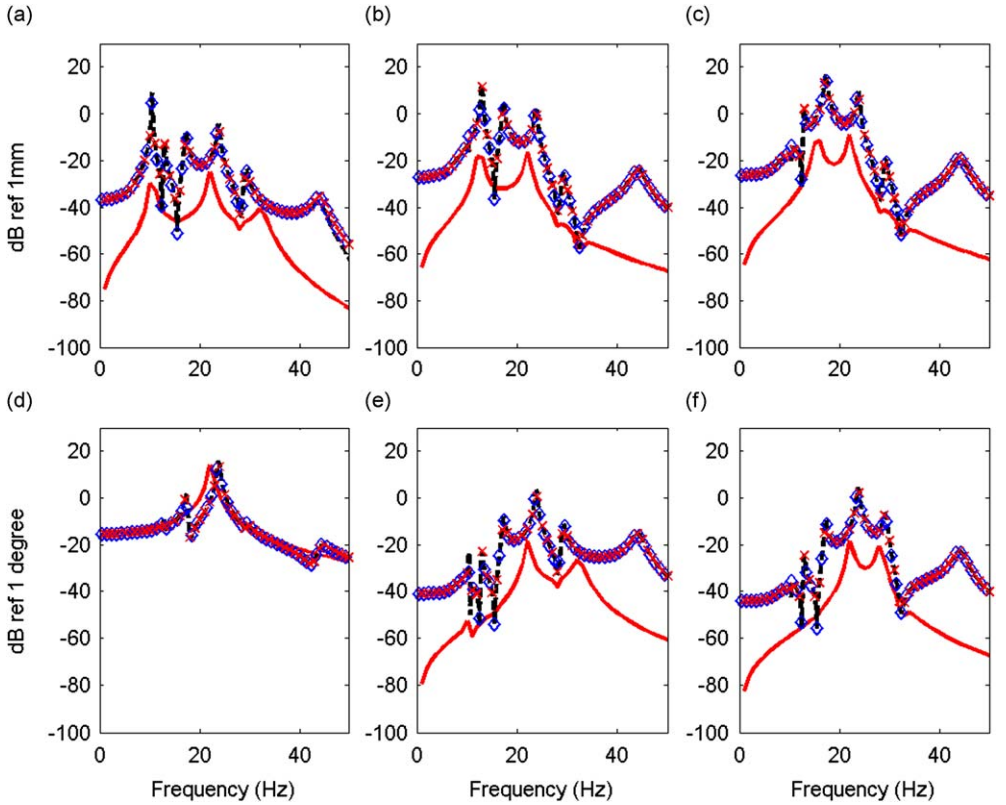

Fig. 5. Frequency response functions predicted by Methods I, II, and III for the powertrain mounting system of Fig. 4 given harmonic torque. One of four mounts is frequency-dependent (hydraulic mount of Fig. 2). (a) $X(\omega)$; (b) $Y(\omega)$; (c) $Z(\omega)$; (d) $\theta_X(\omega)$; (e) $\theta_Y(\omega)$; and (f) $\theta_Z(\omega)$. Key: ▬, high damped mount ($c_{a,1}=10c_a$); ×, Method I (direct inversion method using Voigt model); ▬ ▬, Method II (modal method using transfer function model); and ◆, Method III (modal method using analogous mechanical model).

Table 2
Comparison of calculated and measured natural frequencies of a V6 diesel engine mounting system using both real and complex eigensolutions.

Mode	Natural frequencies (Hz)		
	Measured	Real eigensolution Frequency-independent[a]	Complex eigensolution Frequency-dependent[a]
1	4.17	4.47	4.47
2	5.66	5.97	5.89
3	6.47	7.48	7.35
4	8.76	9.87	9.89
5	12.47	12.27	12.44
6	–	16.45	16.45

A frequency-dependent mount is applied at location #1. Measurements are from Ref. [6].
[a] Properties are shown in Fig. 6.

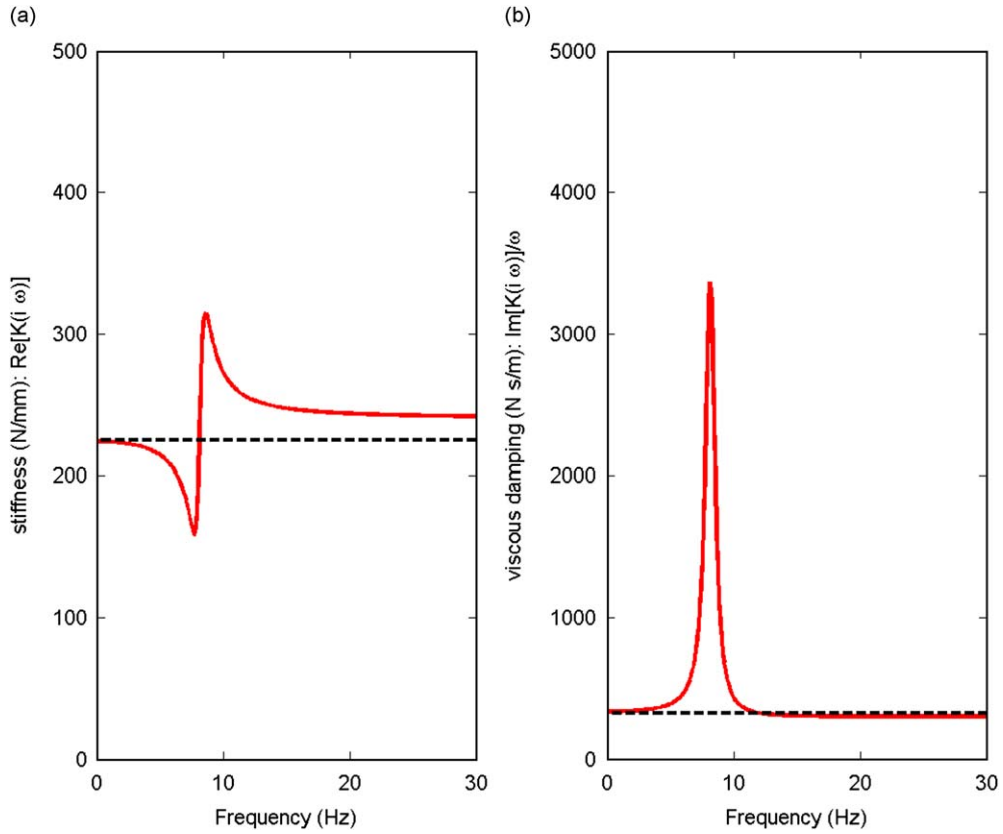

Fig. 6. Spectrally varying stiffness and viscous damping properties of mount #1 when applied to the V6 diesel engine system. (a) Stiffness spectra, $k(\omega) = \mathrm{Re}[K(j\omega)]$; (b) viscous damping spectra, $c(\omega) = \mathrm{Im}[K(j\omega)]/\omega$. Key: ▬, second-order transfer function (TF) modeled by analogous mechanical model of Eq. (3) (with k_r=224 N mm^{-1}, c_r=300 N s m^{-1}, m_M=6.5 kg, c_M=36 N s m^{-1}, and k_M=17 N m^{-1}) for the mount #1; ▬ ▬, zeroth-order transfer function (TF) reported in Ref. [6] for mount #1 (with k=224 N mm^{-1} and c=300 N s mm^{-1}).

6. Nature of eigensolutions

Based on Methods II and III, eigensolutions for the mounting system of Section 5.2 is calculated with a slightly frequency-dependent (rubber) and a highly frequency-dependent (hydraulic) mounts. As shown in Fig. 2, both are modeled by using second-order transfer functions. In Table 3, eigenvalues are compared for frequency-independent rubber and hydraulic mounts. Even though we observe a small change in the eigenvalues for the rubber mount (when compared with the frequency-independent case), a large deviation for the hydraulic mount example is noted, especially near the notch in mount dynamic stiffness spectrum. While the system with constant k and c values has 6 eigenvalues, 7 eigenvalues

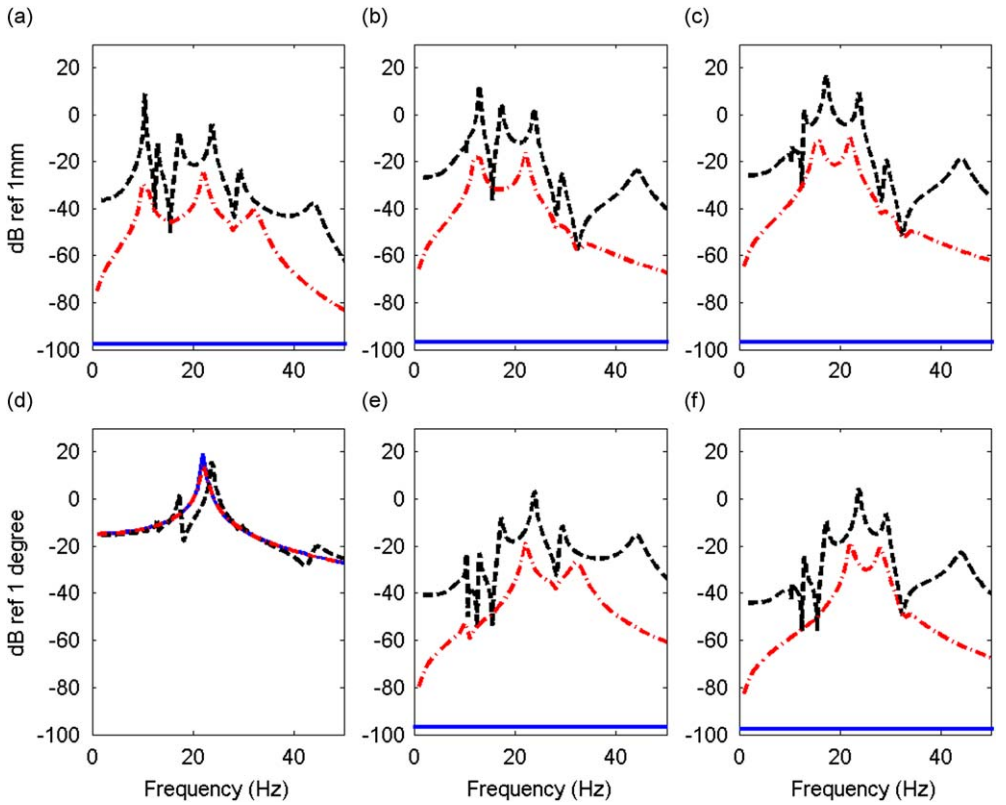

Fig. 7. Motion coupling introduced by a frequency-dependent mount in the powertrain mounting system of Fig. 4. Frequency response functions are compared for 3 cases: frequency-invariant with proportional damping, frequency-invariant with non-proportional damping, and frequency-dependent given harmonic torque. (a) $X(\omega)$; (b) $Y(\omega)$; (c) $Z(\omega)$; (d) $\theta_X(\omega)$; (e) $\theta_Y(\omega)$; and (f) $\theta_Z(\omega)$. Key: ——, proportional damping (frequency-invariant); — —, non-proportional damping (frequency-invariant, $c_{a,1}=10c_a$); and ▬ ▬, frequency-dependent mount (hydraulic mount in Fig. 2).

(one with a high damping ratio (ζ)) are found for the frequency-dependent system. The seventh eigenvalue arises from the hydraulic mount since it is modeled as a second-order system. An additional eigenvector is seen for both transfer function and mechanical models even though the $r_{fd,k}$ element becomes the additional mode component for the transfer function model while the $x_{M,k}$ component is for the mechanical model. Overall, the mechanical model (though approximate) yields a good understanding of the physics.

7. Impulse responses in time domain

Since the proposed rigid body mounting system with spectrally varying mounts generates linear differential equations in the form of Eq. (21) or Eq. (27), it is now possible to analytically calculate the time domain responses using the analytical modal superposition or transition matrix method [23]. Even though either Method II or III can be used for transient analyses, the transfer function model is preferred since it describes the real-life device more accurately than the approximate mechanical model [8]. We calculate the time domain responses for the focalized spectrally varying rigid body mounting system (of Section 5.2) by using Method II given an impulse torque excitation in the x-direction. Impulse responses for a spectrally invariant system are compared as well, though we have replaced the frequency-dependent mount with a highly damped ($10c_a$) rubber mount. Transient responses in Fig. 8 clearly reveal significant coupling in powertrain motions due to the frequency-dependence. Conversely, the impulse responses of Fig. 9 show minimal differences between frequency-independent and rubber (with a minor variation in properties with frequency) mounts as expected.

8. Analysis of coupled motions

8.1. Introduction of coupling from isolators having varying stiffness values

The elastic axis or torque roll axis decoupling scheme is used to decouple the powertrain roll mode [1,2,3,17,24,25] when specific frequency-independent stiffness values are assumed. The focalization method has been widely applied to

Table 3
Complex eigensolutions of the powertrain mounting system of Fig. 4 using the Method II.

Dominant mode	$k \neq k(\omega)$, $c \neq c(\omega)$ Zeroth-order rubber mount		$K(s)$ Second-order rubber mount	
	ω_r (Hz)	ζ (%)	ω_r (Hz)	ζ (%)
(a)				
x	10.4	0.4	10.4	0.1
y	12.5	0.8	12.4	1.4
z	15.5	1.6	15.4	2.4
θ_x	22.2	1.7	22.1	1.9
θ_z	28.2	1.7	28.2	1.8
θ_y	32.3	3.2	32.1	2.9

Dominant mode(s)	$k \neq k(\omega)$, $c \neq c(\omega)$ Zeroth-order hydraulic mount		$K(s)$ Second-order hydraulic mount		
	ω_r (Hz)	ζ (%)	ω_r (Hz)		ζ (%)
(b)					
Mount mode	–	–	8.9	9.0[a]	7.5
x	6.0	0.2	6.0	6.1[a]	0.2
y	7.5	0.3	7.3	7.4[a]	0.1
z (θ_x)	10.0	0.7	11.5	11.2[a]	13.7
θ_x	23.4	1.1	23.5	23.6[a]	1.1
θ_z (θ_y)	29.1	1.2	29.2	29.2[a]	1.1
θ_y (θ_x, θ_z)	41.3	8.4	43.3	43.5[a]	4.6

One of four mounts employs properties of Fig. 2. Resonant frequencies approximated from the frequency response functions as predicted by Method I (direct inversion) are also compared. (a) Rubber mount with m=100.5 kg; (b) hydraulic mount with m=300.5 kg. In each case, eigensolutions with constant properties ($k \neq k(\omega)$, $c \neq c(\omega)$) are also given.

[a] Resonant frequencies from the direct inversion (Method I).

yield only the roll motion under harmonic torque excitation. In this method, constant principal compressive stiffness (k_a) and its ratio (L_k=k_a/k_b) to the principal shear stiffness (k_b) values are selected to place the elastic center at the center of gravity to avoid both static and dynamic couplings. However, the introduction of spectrally varying stiffness in the principal compressive direction results in altering the stiffness ratio (L_k), and thus, it would induce varied coupling at each frequency. To illustrate the significance of this problem, a simple 2-D mounting system of Fig. 10 is analyzed first. The mounting system parameters for the roll mode decoupling are chosen as follows: mass m=70 kg; moment of inertia (kg m^2) I_{XX}=20 kg m^2; principal compressive stiffness k_a=840 N mm^{-1}; stiffness rate ratio L_k(=k_a/k_b)=5.8; mount orientation ϕ=22.5°; mount location r_y=r_z=0.3 m. The principal compressive stiffness is changed from the nominal value of k_a to 4k_a, 0.7k_a, and 0.2k_a, respectively, to describe a range of frequency-dependent values. The elastic center (CE) is defined as the origin of the elastic axis coordinate system where no static coupling exists. For the focalized plane mounting scheme, CE is calculated by the following:

$$\frac{r_z - r_{z,e}}{r_y} = \frac{(L_k - 1)\tan\phi}{L_k \tan^2\phi + 1}. \tag{35}$$

Fig. 11 shows the CE coordinates corresponding to a range of k_a values. It is noted that as k_a deviates from the targeted value for roll mode decoupling, further CE moves away from the center of gravity (CG). The extent of coupling among the motions is also displayed in Table 4 in terms of the modal kinetic energy fraction [26] at the roll natural frequency (this will be discussed in detail in the Section 8.2). The energy fraction matches very well with the CE coupling measure of Fig. 11. Corresponding frequency responses (given harmonic torque excitation) are shown in Fig. 12; refer to Fig. 10 for the identification of symbols. The decoupled roll motion is now coupled since the stiffness ratio L_k changes due to a change in k_a. In addition, high damping coefficient over a certain frequency range (intentionally chosen to control certain powertrain system resonance(s)) induces further coupling among the powertrain motions; this is partially due to an introduction of non-proportional damping as reported by Park and Singh [3]. Results for a simple mounting system suggest that we need to further investigate the effect of spectrally varying mounts on coupling between powertrain motions and in particular torque roll axis decoupling schemes [2,3].

8.2. Modal kinetic energy distribution based on complex eigensolutions

Even though the modal kinetic energy is conventionally defined for real eigensolutions [26] as used in the previous section, coupling between motions for a spectrally varying system should be quantified in terms of the complex modes;

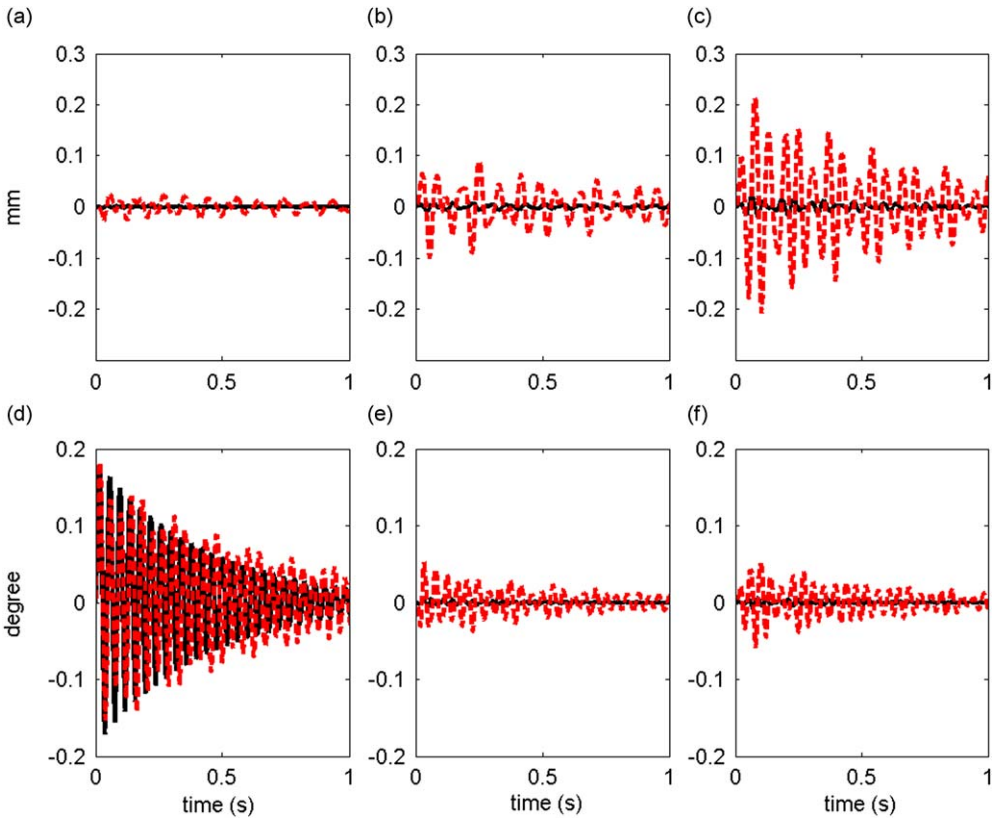

Fig. 8. Impulse responses for the powertrain mounting system of Fig. 4 given torque excitation. One of four mounts is replaced by a frequency-dependent hydraulic (or by a highly damped) mount. (a) $x(t)$; (b) $y(t)$; (c) $z(t)$; (d) $\theta_x(t)$; (e) $\theta_y(t)$; and (f) $\theta_z(t)$. Key: ▬ ▬, frequency-dependent mount (hydraulic mount in Fig. 2) and ▬, highly damped mount ($c_{a,1} = 10c_a$).

recall the eigensolutions for the spectrally varying mounting systems based on Method II or III. Define the modal kinetic energy scalar function, ξ_{X_i,ω_r}, in the X_i direction, at a natural frequency ω_r, (for a spectrally varying symmetric powertrain system based on Method II) as follows, where KE_{X_i,ω_r} and KE_{ω_r} could be defined based on either right or adjoint eigenvector:

$$\xi_{X_i,\omega_r} = \frac{KE_{X_i,\omega_r}}{KE_{\omega_r}}, \tag{36}$$

First, using the right eigenvector, define

$$KE_{X_i,\omega_r} = \frac{1}{2}[\mathbf{M}]_{ii}\omega_r^2\left|[\mathbf{u}_r]_{X_i}\right|^2 \text{ and } KE_{\omega_r} = \frac{1}{2}\omega_r^2\left|\mathbf{u}_r^{\mathrm{T}}\mathbf{M}\mathbf{u}_r\right|, \tag{37a}$$

Second, using the left (adjoint) eigenvector, define

$$KE_{X_i,\omega_r} = \frac{1}{2}[\mathbf{M}]_{ii}\omega_r^2\left|[\mathbf{v}_r]_{X_i}\right|^2 \text{ and } KE_{\omega_r} = \frac{1}{2}\omega_r^2\left|\mathbf{v}_r^{\mathrm{T}}\mathbf{M}\mathbf{v}_r\right|. \tag{37b}$$

Here, $[\mathbf{u}_r]_{X_i}$ is the X_i-direction component of the r-th mode. Using Eqs. (37a, b), Table 5 compares the modal scalar distributions for the powertrain system with one hydraulic and three rubber mounts (as discussed in the Section 5.2). The modal energy distributions from Method III are also compared with those from Method II in Table 5. Observe that Method II (with right eigenvectors) and Method III yield the same distributions. Therefore, Method III could be utilized to calculate the modal kinetic energies for a spectrally varying dynamic system.

8.3. *Roll mode decoupling with frequency-dependent mounts*

Prior work [2] shows that the roll mode in a simple focalized mounting system (under torque excitation as shown in Figs. 1 and 4) can be decoupled by satisfying the following condition:

$$\frac{r_z}{r_y} = \frac{(L_k - 1)\tan\phi}{L_k\tan^2\phi + 1}. \tag{38}$$

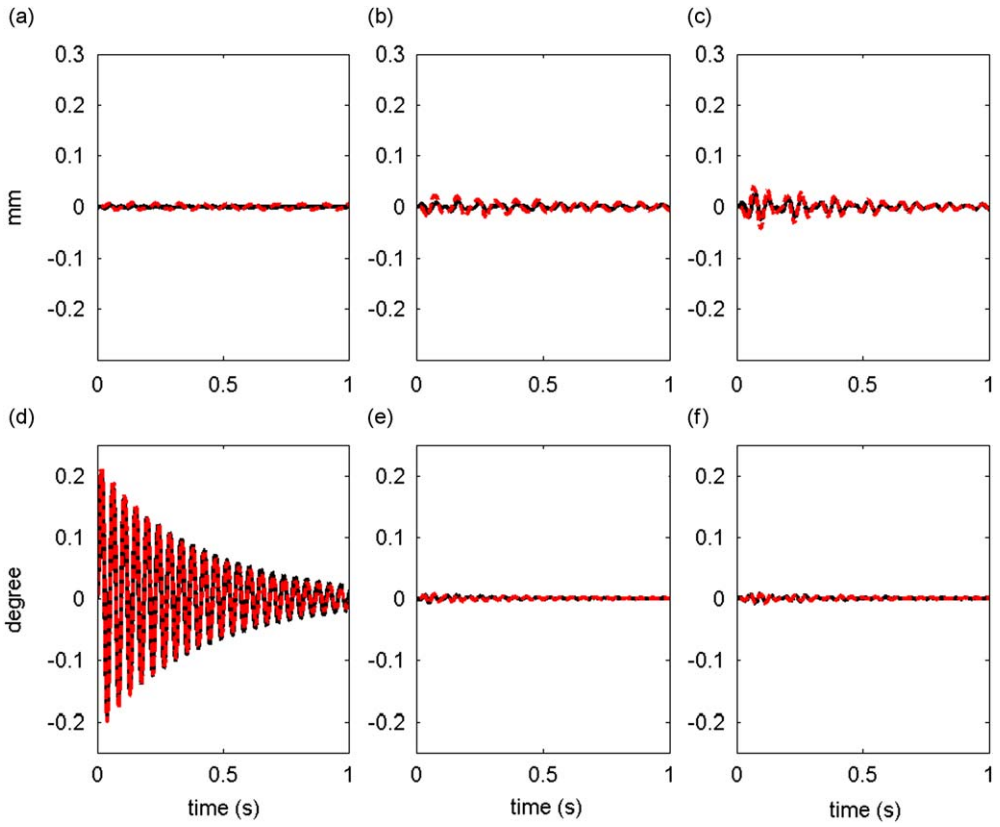

Fig. 9. Impulse responses for the powertrain mounting system of Fig. 4 given torque excitation. One of four mounts is replaced by a frequency-dependent rubber (or a highly damped) mounts. (a) $x(t)$; (b) $y(t)$; (c) $z(t)$; (d) $\theta_x(t)$; (e) $\theta_y(t)$; and (f) $\theta_z(t)$. Key: ▬ ▬, frequency-dependent mount (rubber mount in Fig. 2) and ▬, highly damped mount ($c_{a,1} = 10c_a$).

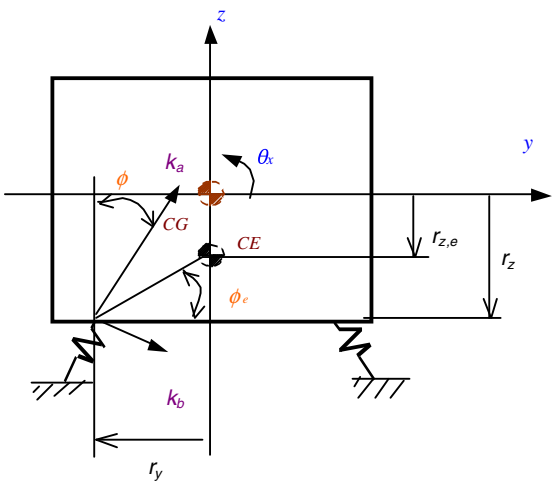

Fig. 10. Focalized 3-dof powertrain mounting system. Here, CG is the center of gravity, CE is the elastic center, k_a is the principal compressive stiffness, and k_b is the principal shear stiffness.

Accordingly, the 6-dof powertrain isolation system is reduced to the following single dof model:

$$I_{XX}\ddot{\theta}_X(t) + k_{\theta_X\theta_X}\theta_X(t) = T(t), \tag{39}$$

where, $k_{\theta_X\theta_X} = 4k_a r_y^2(1/L_k \sin^2\phi + \cos^2\phi)$. Thus the torque, $T(t)$, excites only the roll motion as no coupling is observed in Eq. (39). In order to analyze the effect of spectrally varying mounts on coupling, two frequency-dependent hydraulic

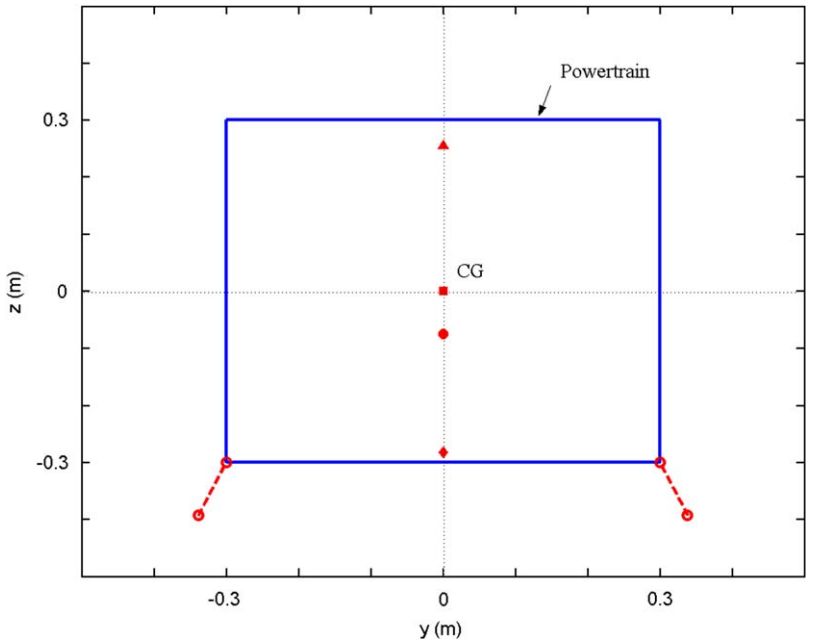

Fig. 11. Coordinates of the elastic center (CE) of the 3-dof powertrain mounting system (Fig. 10), as the values of principal compressive stiffness (k_a) of both mounts are varied. Key: ▲, $4k_a$; ■, k_a (nominal value=840 N mm^{-1}); ●, $0.7k_a$; and ◆, $0.2k_a$.

Table 4
Modal kinetic energy fraction (ξ) and elastic center (CE) locations as decoupling indices for the 3-dof powertrain mounting system of Fig. 10.

$k_{a,1}(=k_{a,2})$ value	ξ at the roll (θ_x) mode (%)			|CE−CG| (m)
	y	z	θ_x	
$4k_a$	31.9	0	68.1	0.25
k_a	0	0	100.0	0
$0.7k_a$	10.1	0	89.9	0.08
$0.2k_a$	33.5	0	66.5	0.29

Here, CE is the elastic center, CG is the center of gravity, and k_a=840 N mm^{-1} is the nominal value.

mounts of Fig. 2 (with mechanical models as shown in Fig. 3(b)) are placed at locations #1 and #2; their internal rubber parts have the same properties as the other two rubber mounts with constants k and c. By using the proposed frequency-dependent mounting system model, the new governing equation in the roll direction (θ_X) is derived as follows:

$$I_{XX}\ddot{\theta}_X(t)+k_{\theta_X Y}y(t)+(k_{\theta_X\theta_X}+k'_{\theta_X\theta_X})\theta_X(t)+k_{\theta_X\theta_Z}\theta_Z(t)+k_{\theta_X fd}x_{M,1}-k_{\theta_X fd}x_{M,2}=T(t), \tag{40}$$

where,

$$k_{\theta_X Y}=-2k_M r_y\frac{\cos\phi\sin\phi}{L_k\sin^2\phi+\cos^2\phi}, \tag{41a}$$

$$k'_{\theta_X\theta_X}=2k_M r_y\frac{\cos^2\phi}{(L_k\sin^2\phi+\cos^2\phi)^2}, \tag{41b}$$

$$k_{\theta_X\theta_Z}=-2k_M r_x r_y\frac{\cos\phi\sin\phi}{L_k\sin^2\phi+\cos^2\phi}, \tag{41c}$$

$$k_{\theta_X fd}=k_M r_y\frac{\cos\phi}{L_k\sin^2\phi+\cos^2\phi}. \tag{41d}$$

A comparison of Eq. (40) with Eq. (39) shows that $T(t)$ excites not only the roll motion (θ_X) but also lateral (y) and yaw (θ_Z) motions. In addition, the inertia track masses in both hydraulic mounts are also excited (in terms of $x_{M,1}$ and $x_{M,2}$) due

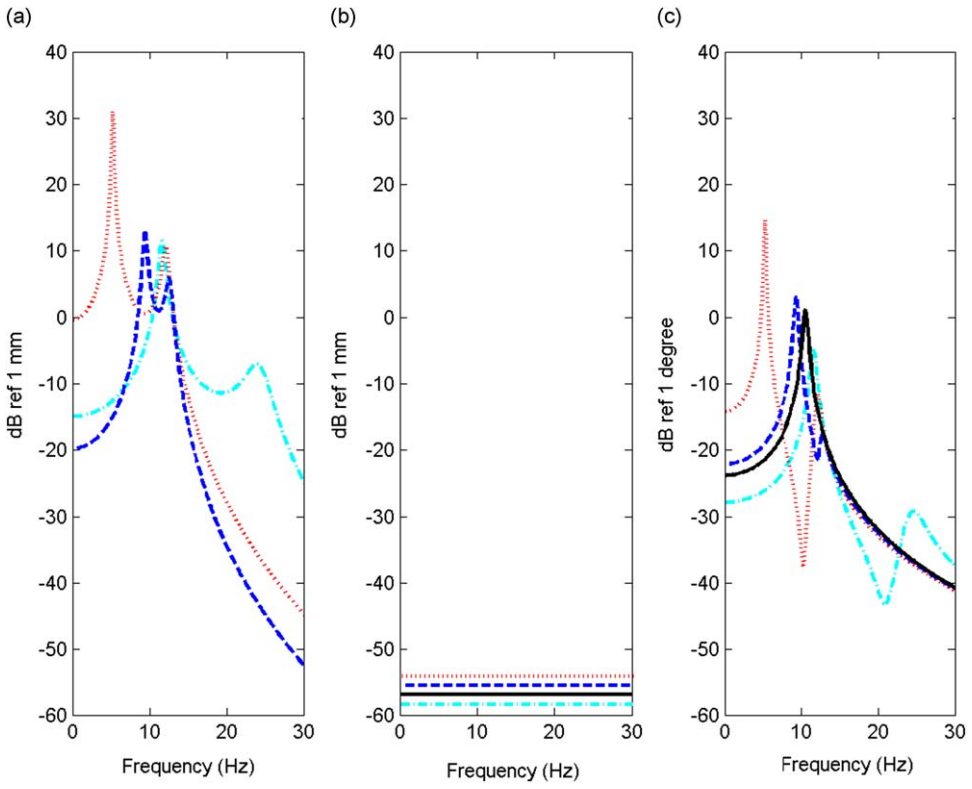

Fig. 12. Frequency response functions of the 3-dof powertrain mounting system of Fig. 10 given harmonic torque. The values of principal compressive stiffness, k_a, of both mounts are varied. (a) $Y(\omega)$; (b) $Z(\omega)$; and (c) $\theta_X(\omega)$. Key: ▬ ▪ ▬, $4k_a$; ▬, k_a (nominal value = 840 N mm^{-1}): TRA-decoupled (focalized); ▬ ▬, $0.7k_a$; and ▪ ▪ ▪, $0.2k_a$.

Table 5
Modal kinetic energy fractions (ξ_{ω_r}) of the powertrain mounting system of Fig. 4 using three methods.

ω_r (Hz)	ξ_{ω_r} (%)						
	9.7	10.4	13.0	17.3	23.8	29.2	44.1
x	6*, 6**, 0***	99, 99, 93	0, 0, 0	0, 0, 0	0, 0, 0	0, 0, 0	0, 0, 1
y	40, 40, 6	0, 0, 1	91, 91, 56	5, 5, 1	1, 1, 0	0, 0, 0	1, 1, 2
z	38, 38, 14	0, 0, 1	8, 8, 16	82, 82, 29	3, 3, 0	1, 1, 0	5, 5, 5
θ_x	8, 8, 16	0, 0, 1	1, 1, 6	10, 10, 25	80, 80, 48	2, 2, 0	8, 8, 3
θ_y	5, 5, 49	0, 0, 3	0, 0, 16	2, 2, 33	6, 6, 30	22, 22, 38	71, 71, 84
θ_z	3, 3, 16	0, 0, 1	0, 0, 5	2, 2, 13	9, 9, 21	76, 76, 61	14, 14, 5

Here, Method II uses both right or adjoint eigenvalue formulations, and Method III employs the mechanical model.
Key to the sequence: *, Method III; **, Method II with right eigenvalue problem; ***, Method II with adjoint eigenvalue problem.

to the coupling term given by $k_{\theta_X fd}$. All of the coupling terms in Eqs. (41a–d) vanish when the inertia track induced stiffness, k_M, is set to zero.

Frequency responses are calculated next for a focalized mounting system with two frequency-dependent mounts (described in the Section 5.2) under harmonic torque excitation with the following system parameters: Mass m=276.7 kg; moment of inertia (kg m^2) I_{XX}=15.8, I_{YY}=11.64, I_{ZZ}=15.69; and inertia product (kg m^2) $I_{XY}=I_{XZ}=I_{YZ}=0$. Stiffness and damping coefficients of the rubber mounts are: stiffness $k_a=k_r$; stiffness rate ratio $L_k(=k_a/k_b)=2.5$; damping $c_a=c_r$; damping rate ratio $L_c(=c_a/c_b)=2.5$; mount orientation, $\phi=15^\circ$; $r_{x,1}=r_{x,2}=318$ mm, $r_{x,3}=r_{x,4}=-318$ mm; $r_{y,1}=r_{y,2}=-198$ mm, $r_{y,2}=r_{y,4}=198$ mm; $r_{z,1}=r_{z,2}=r_{z,3}=r_{z,4}=-68$ nm. Note that resultant frequency responses are coupled as shown in Fig. 13. The roll mode decoupling is achieved by placing the elastic center projection line (obtained from the elastic centers of two symmetric mounts, respectively, #1 and #2, and likewise #3 and #4) on the torque (roll) axis direction (x-direction). Based on Eqs. (41a) and (41c), it is found that an orientation angle of 0° does indeed decouple the motions, even with spectrally

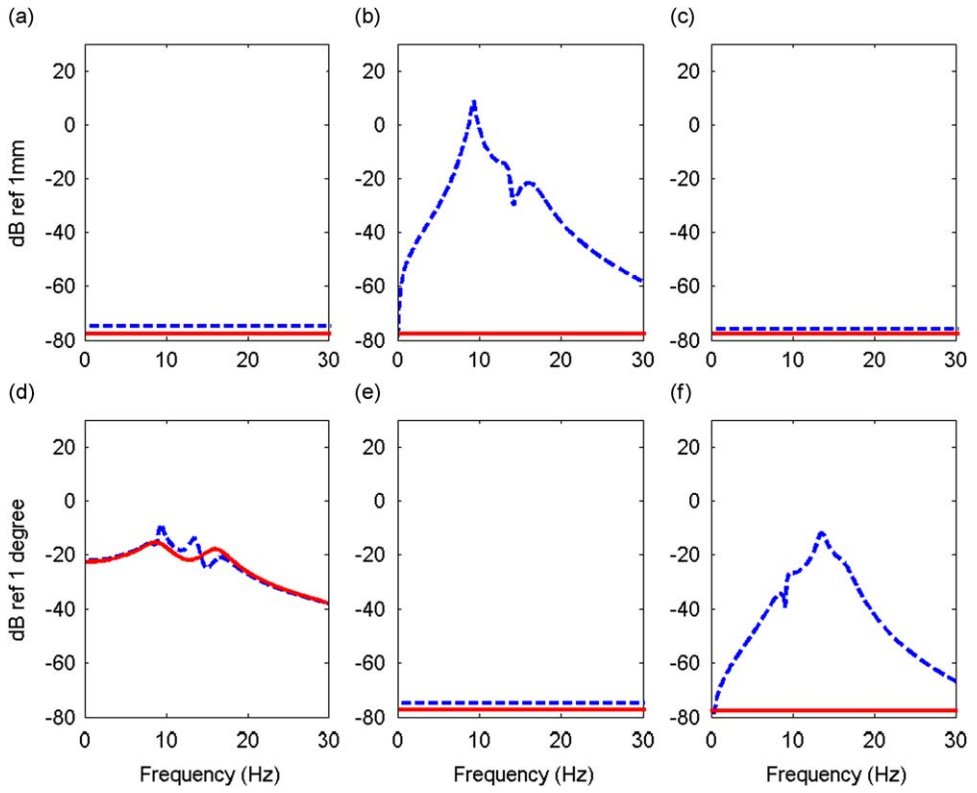

Fig. 13. Comparison of decoupled frequency response functions with coupled functions for a powertrain mounting system of Fig. 4 given harmonic torque. Two spectrally varying mounts of hydraulic mount in Fig. 2 are applied at locations #1 and #2. Mount parameters (orientation angle, ϕ and vertical location, r_z) are chosen for TRA decoupling. (a) $Y(\omega)$; (b) $Z(\omega)$; (c) $Z(\omega)$; (d) $\theta_X(\omega)$; (e) $\theta_Y(\omega)$; and (f) $\theta_Z(\omega)$. Key: ▬ ▬, coupled ($\phi=15^\circ$ and $r_z=-68$ mm); and ▬, TRA-decoupled ($\phi=0^\circ$ and $r_Z=0$ mm).

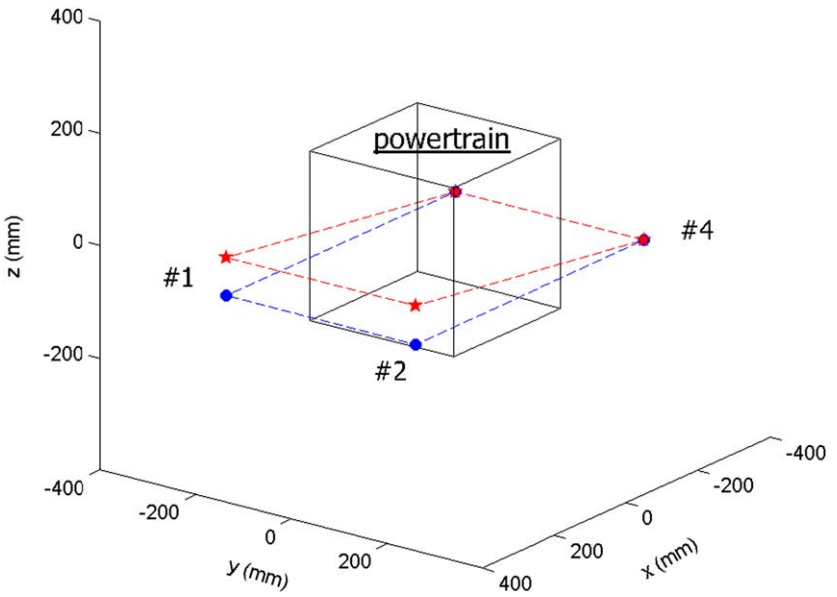

Fig. 14. Mount locations for coupled and decoupled powertrain of Fig. 4 given harmonic torque excitation. Two frequency-dependent mounts are placed at locations #1 and #2 and the rest (locations #3 and #4) are frequency-independent mounts; motions are decoupled by adjusting locations and orientation angle of mounts. Key: ★, TRA decoupled ($\phi=0^\circ$ and $r_z=0$ mm); and ●, coupled ($\phi=15^\circ$ and $r_z=-68$ mm).

Table 6
Modal kinetic energy fractions (ξ) of the powertrain mounting system of Fig. 4 for coupled and decoupled cases.

Coupling scheme	ξ (%) at the roll (θ_x) mode (9.3 Hz)					
	x	y	z	θ_x	θ_y	θ_z
Coupled ($\phi_1=\phi_2=15^\circ$, $r_{z,1}=r_{z,2}=-68$ mm)	0	88.5	0	11.3	0	0.2
TRA-decoupled ($\phi_1=\phi_2=0^\circ$, $r_{z,1}=r_{z,2}=-68$ mm)	0	0	0	100	0	0

Spectrally varying hydraulic mounts of Fig. 2 are placed at locations #1 and #2, respectively. Mount parameters (orientation angle, ϕ, and vertical location, r_z) are appropriately chosen to decouple or couple the TRA mode.

varying mount properties; note that when $\phi=0^\circ$, r_Z is found to be 0 for a focalized mounting scheme. Frequency responses of this decoupled mounting scheme are shown in Fig. 13, and the corresponding mount locations are illustrated in Fig. 14. Table 6 compares the modal kinetic energy distributions at the roll mode for both coupled and TRA-decoupled systems with frequency-dependent mounts. Recall that the roll mode was severely coupled with lateral (y) direction with frequency-dependent mounts; it is now decoupled, thereby resulting in 100% energy content in the roll direction (θ_X) alone.

9. TRA decoupling of spectrally varying powertrain mounting system

Recall from Eq. (29) that the eigenvectors of direct and adjoint eigenvalue problems for a spectrally varying mounting system are biorthogonal with respect to **A** and **B**. Based on this biorthogonal property, we analytically show that the torque roll axis decoupling for a spectrally varying mounting system could still be achieved; proof is as follows. Apply the harmonic torque excitation to Eqs. (21) and (22) as $\mathbf{f}_e(t)=\mathbf{T}_e e^{j\omega t}$ where $\mathbf{T}_e=[\mathbf{T}^T,(\mathbf{M}_{fd}\boldsymbol{\eta})^T]^T$; also, define $\mathbf{f}(t)=\mathbf{T}e^{i\omega t}$, $\boldsymbol{\sigma}(t)=\mathbf{M}_{fd}\boldsymbol{\eta}e^{i\omega t}$, and $\boldsymbol{\eta}=\left[\eta_1,\eta_2,\ \ldots,\ \eta_{N_{fd}}\right]^T$ where η_i are constants. Then the steady-state response will be in the form of $\mathbf{q}_e(t)=\left[\mathbf{q}^T,q_1,q_2,\ \ldots,\ q_{N_{fd}}\right]^T(t)e^{j\omega t}=\mathbf{Q}_e e^{j\omega t}$, leading to

$$j\omega\mathbf{AP}+\mathbf{BP}=\mathbf{G}, \tag{42}$$

$$\mathbf{G}=\begin{bmatrix}\mathbf{T}_e\\ \mathbf{0}\end{bmatrix},\quad \mathbf{P}=\begin{bmatrix}j\omega\mathbf{Q}_e\\ \mathbf{Q}_e\end{bmatrix}. \tag{43a,b}$$

Based on the orthogonal property of eigenvectors, the dynamic response of the 6-dof system is expressed by $\mathbf{P}=\sum_{r=1}^{2N}b_r\mathbf{U}_r$ where, $\mathbf{U}_r$ is the eigenvector and b_r is the modal participation coefficient. The orthogonal property of the complex eigenvectors provides the following relations: $\mathbf{V}_r^T\mathbf{A}\mathbf{U}_s=\delta_{rs}$, $\mathbf{V}_r^T\mathbf{B}\mathbf{U}_s=-\lambda_r\delta_{rs}$, $r,s=1,2,\ \ldots,\ 2(N+N_{fd})$. Using the above properties, Eq. (42) yields

$$b_r=\frac{\mathbf{V}_r^T\mathbf{G}}{j\omega-\lambda_r}. \tag{44}$$

In order to achieve the roll mode motion decoupling, it is assumed that one of the eigenvectors must be parallel to the torque roll axis (TRA) direction. Define the torque roll axis direction, $\mathbf{q}_{e,TRA}$, and let one mode, $\mathbf{u}_s$, be in the torque roll axis direction as follows where γ and ρ are scalar constants:

$$\mathbf{q}_{e,TRA}=\begin{bmatrix}\mathbf{q}_{TRA}\\ \boldsymbol{\eta}\end{bmatrix}=\begin{bmatrix}\gamma\mathbf{M}^{-1}\mathbf{T}\\ \boldsymbol{\eta}\end{bmatrix}, \tag{45}$$

$$\mathbf{U}_s=\rho\mathbf{P}_{e,TRA},\ \text{where}\ \mathbf{U}_s=\begin{bmatrix}\lambda\mathbf{u}_s\\ \mathbf{u}_s\end{bmatrix}\ \text{and}\ \mathbf{P}_{e,TRA}=\begin{bmatrix}\lambda\mathbf{q}_{e,TRA}\\ \mathbf{q}_{e,TRA}\end{bmatrix}. \tag{46}$$

Combining Eqs. (45) and (46) and using

$$\mathbf{V}_r^T\mathbf{A}\mathbf{U}_s=\rho\mathbf{V}_r^T\begin{bmatrix}\mathbf{M}_e & \mathbf{0}\\ \mathbf{0} & -\mathbf{K}_e\end{bmatrix}\begin{bmatrix}\lambda\mathbf{q}_{e,TRA}\\ \mathbf{q}_{e,TRA}\end{bmatrix},$$

we obtain

$$\mathbf{V}_r^T\mathbf{G}=\frac{1}{\rho\gamma}\frac{1}{\lambda}\left(\mathbf{V}_r^T\mathbf{A}\mathbf{U}_s+\mathbf{V}_r^T\begin{bmatrix}\mathbf{0}\\ \mathbf{K}\mathbf{u}_s\end{bmatrix}\right);\quad r,s=1,2,3,\ \ldots,\ 2(N+N_{fd}). \tag{47a}$$

Expand the above to yield

$$\mathbf{V}_r^{\mathrm{T}}\mathbf{G} = \frac{1}{\rho\gamma}\frac{1}{\lambda}(\delta_{rs} + \mathbf{v}_r^{\mathrm{T}}\mathbf{K}\mathbf{u}_s). \tag{47b}$$

Since $\mathbf{u}_s$ is set in the torque roll axis direction, Eqs. (47a, b) become

$$\mathbf{V}_r^{\mathrm{T}}\mathbf{G} = \frac{1}{\rho\gamma}(1 + a_s)\delta_{rs}. \tag{47c}$$

Here $a_s = \mathbf{v}_s^{\mathrm{T}}\mathbf{K}\mathbf{u}_s$. From Eqs. (44) and (47c), only $b_s \neq 0$ and $b_r = 0$. Eventually, the forced response, $\mathbf{q}(t)$, exists only in the torque roll axis direction for a frequency-dependent dynamic system.

When we include a mechanical mount model in the isolation system, Eq. (27) is transformed into state space form as follows:

$$\mathbf{A}_M\dot{\mathbf{p}}_M(t) + \mathbf{B}_M\mathbf{p}_M(t) = \mathbf{g}_M(t), \tag{48}$$

$$\mathbf{A}_M = \begin{bmatrix} \mathbf{M}_{Me} & \mathbf{0} \\ \mathbf{0} & -\mathbf{K}_{Me} \end{bmatrix}, \quad \mathbf{B}_M = \begin{bmatrix} \mathbf{C}_{Me} & \mathbf{K}_{Me} \\ \mathbf{K}_{Me} & \mathbf{0} \end{bmatrix}, \quad \mathbf{p}_M(t) = \begin{bmatrix} \dot{\mathbf{q}}_{Me}(t) \\ \mathbf{q}_{Me}(t) \end{bmatrix}, \quad \mathbf{g}_M(t) = \begin{bmatrix} \mathbf{f}_{Me}(t) \\ \mathbf{0} \end{bmatrix}. \tag{49a,b,c,d}$$

The resultant complex eigenvectors are orthogonal with respect to $\mathbf{A}_M$ and $\mathbf{B}_M$ since the system matrices $\mathbf{M}_{Me}$, $\mathbf{K}_{Me}$, and $\mathbf{C}_{Me}$ are symmetric, unlike those for Method II. Accordingly, we can apply the procedure suggested by Park and Singh [3] for a non-proportionally damped system. The forced motion, $\mathbf{q}(t)$, exists only in the torque roll axis direction as long as a mode is in the torque roll axis direction.

10. Conclusion

In this article, three methods for representing mounts with $k(\omega)$ and $c(\omega)$ are critically examined in describing the eigensolutions and frequency responses of an isolation system. Table 1 summarizes and compares Methods I, II, and III by assuming that the hydraulic mounts of Fig. 2 (with a dimension of N_{hyd}) are embedded in a 6-dof isolation system. To overcome the deficiencies of Method I (limited to only the frequency domain analysis), Methods II and III are developed by employing transfer function (in Laplace domain) and mechanical system formulations, respectively. Both analytical methods compare well with the direct inversion method in predicting the frequency responses. Impulse response is also analytically calculated based on the proposed methods.

The powertrain motion coupling issues are investigated under harmonic or impulse torque excitation. New coupling indices, including modal kinetic energy fractions, are defined for Methods II and III, and they are found to be useful in the analysis of spectrally varying mounting systems. Even though the roll mode decoupled mounting scheme (by using the focalization method under harmonic torque excitation) can be represented by a reduced single dof model, additional dof is introduced by the hydraulic mount and consequently the roll mode is coupled again with lateral and yaw motions. Nonetheless, the roll mode could still be decoupled (in the focalized mounting scheme) by placing the mounts with $k(\omega)$ and $c(\omega)$ in the vertical direction and located at the same height as the center of gravity of powertrain. By employing direct and adjoint eigenvalue problems in Method II, it has been shown that the TRA decoupling with frequency-dependent elements is possible provided a mode is always set in the TRA direction. However, detailed numerical examples and design studies are left for future work. Note that two eigenvalue problems in terms of stiffness and viscous damping matrices need to be solved for systems with $k(\omega)$ and $c(\omega)$. An investigation of the effect of amplitude-sensitive mount on motion coupling should be pursued in future work along with an examination of the role of flexible base (say with few modes) over the lower frequency range.

Acknowledgments

We are grateful to the member organizations of the Smart Vehicle Concepts Center (www.SmartVehicleCenter.org) and the National Science Foundation Industry/University Cooperative Research Centers program (www.nsf.gov/eng/iip/iucrc) for supporting this work.

References

[1] C.M. Harris, *Shock and Vibration Handbook*, McGraw-Hill, New York, 1995 (Chapter 3).
[2] T. Jeong, R. Singh, Analytical methods of decoupling the automotive engine torque roll axis, *Journal of Sound and Vibration* 234 (2000) 85–114.
[3] J. Park, R. Singh, Effect of non-proportional damping on the torque roll axis decoupling of an engine mounting system, *Journal of Sound and Vibration* 313 (2008) 841–857.
[4] H. Ashrafiuon, Design optimization of aircraft engine mount Systems, *ASME Journal of Vibration and Acoustics* 115 (4) (1993) 463–467.
[5] H. Ashrafiuon, C. Nataraj, Dynamic analysis of engine-mount systems, *ASME Journal of Vibration and Acoustics* 14 (1) (1992) 79–83.
[6] C.E. Spiekermann, C.J. Radcliffe, E.D. Goodman, Optimal design and simulation of vibrational isolation systems, *Journal of Mechanisms Transmissions and Automation in Design* 107 (1985) 271–276.
[7] J.S. Tao, G.R. Liu, K.Y. Lam, Design optimization of marine engine-mount system, *Journal of Sound and Vibration* 235 (2000) 477–494.

[8] R. Singh, G. Kim, P.V. Ravindra, Linear analysis of automotive hydro-mechanical mount with emphasis on decoupler characteristics, *Journal of Sound and Vibration* 158 (1992) 219–243.
[9] M.L. Tinker, M.A. Cutchins, Instabilities in a non-linear model of a passive damper, *Journal of Sound and Vibration* 176 (1994) 415–428.
[10] E.I. Rivin, *Passive Vibration Isolation*, ASME Press, New York, 2003.
[11] R.A. Ibrahim, Recent advances in nonlinear passive vibration isolators, *Journal of Sound and Vibration* 314 (2008) 371–452.
[12] Y. Yu, N.G. Naganathan, R.V. Dukkipati, Review of automotive vehicle engine mounting systems, *International Journal of Vehicle Design* 24 (4) (2000) 299–319.
[13] S. He, R. Singh, Estimation of amplitude and frequency dependent parameters of hydraulic engine mount given limited dynamic stiffness measurements, *Noise Control Engineering Journal* 53 (6) (2005) 271–285.
[14] T. Jeong, R. Singh, Inclusion of measured frequency- and amplitude-dependent mount properties in vehicle or machinery models, *Journal of Sound and Vibration* 245 (2001) 385–415.
[15] S.H. Crandall, The role of damping in vibration theory, *Journal of Sound and Vibration* 11 (1970) 3–18.
[16] J.P. Den Hartog, *Mechanical Vibrations*, Dover Publications, New York, 1985.
[17] J. Bang, H. Yoon, K. Won, Experiment and simulation to improve key on/off vehicle vibration quality, Society of Automotive Engineering Paper 2007-01-2363 (2007).
[18] H. Adiguna, M. Tiwari, R. Singh, H.E. Tseng, D. Hrovat, Transient response of hydraulic engine mount, *Journal of Sound and Vibration* 268 (2003) 217–248.
[19] A. Papoulis, *The Fourier Integral and its Applications*, McGraw-Hill, New York, 1962.
[20] J.H. Lee, K.J. Kim, Treatment of frequency-dependent complex stiffness for commercial multi-body dynamic analysis programs, *Mechanics of Structures and Machines* 30 (4) (2002) 527–541.
[21] J.S. Bendat, A.G. Piersol, *Random Data*, John Wiley & Sons, New York, 2000.
[22] J.H. Lee, R. Singh, Critical analysis of analogous mechanical models used to describe hydraulic engine mounts, *Journal of Sound and Vibration* 311 (2008) 1457–1464.
[23] L. Meirovitch, *Principles and Techniques of Vibrations*, Prentice Hall, New Jersey, 1997.
[24] B.J. Kim, Three dimensional vibration using elastic axes, M.S. thesis, Michigan State University, 1991.
[25] D. FitzGerald, Focused engine isolation systems—The benefits, Society of Automotive Engineering Paper 972777 (1997).
[26] S. Johnson, J. Subhedar, Computer optimization of engine mounting systems, Society of Automotive Engineering Paper 790974 (1979).